

Solidification of metal foams

M. Mukherjee^{1,2,*}, F. Garcia-Moreno^{1,2}, J. Banhart^{1,2}

¹Helmholtz-Zentrum Berlin, Hahn-Meitner-Platz, 14109 Berlin, Germany

²Technische Universität Berlin, Hardenbergstrasse 36, 10623 Berlin, Germany

Abstract

Expansion and contraction phenomena during solidification of liquid metal foams were studied. Such foams were processed by mixing metal powders with TiH₂ powder and compacting the resulting blends, after which the compacted powders were melted. The subsequent foaming process was monitored *in-situ* by X-ray radioscopy. An intermediate expansion stage during solidification was observed. This solidification expansion (SE) could be linked with phase transformations in the alloy. SE was found to depend mainly on the time spent at the foaming temperature before cooling (holding time), the cooling rate and the alloy composition. The interplay between gas shrinkage, solidification shrinkage, gas production by the blowing agent and gas losses due to out-diffusion was identified as the main reason for SE. While the blowing agent had a major influence on SE, gas dissolved in the metal also played a role, since some SE was observed in foams blown without TiH₂ by pure pressure manipulation.

Keywords: metal foam, solidification expansion, phase transformation, blowing agent, diffusion

* Corresponding author: M. Mukherjee. Phone: +49 30 8062 2820. Fax: +49 30 8062 3059. E-mail: manas.mukherjee@gmail.com

1. Introduction

Significant progress in metal foam research has been made in the past two decades although a detailed understanding of foaming is still lacking. Various aspects of the physics of metal foaming have been investigated, including the characteristics of the gas source [1–3], early stages of pore formation [4], evolution of metal foam [5,6], drainage of liquid metal [7], coalescence [5,7–9], foam stabilization [10–11] and the influence of ambient atmosphere [11–13] and pressure [3,13]. Foams in engineering applications are in the solid state, and liquid metal foam is merely a stage that occurs during processing. Although solidification is an essential and unavoidable processing step that all liquid metal foams have to go through, only very few studies have been carried out, including work on the change in porosity [14], the development of drainage [15] and the occurrence of coalescence [8] during solidification of metal foam.

In the present study, the evolution of metal foams during solidification was investigated. The macroscopic expansion and contraction during cooling was studied *in-situ* by means of X-ray radiography. The main topic of this study is the expansion stage observed during solidification that appears *anomalous* since at first sight one would expect contraction of the foam throughout solidification. The effect is technologically relevant since it has an impact on the manufacture of engineering components in moulds [12] and large foam products [16]. The discovery of the effect has been reported by the present authors [17]. In this article, an extensive experimental study is presented, and the mechanisms behind the anomalous expansion behaviour are discussed in detail in the light of alloy solidification and blowing agent decomposition.

2. Experimental

2.1. Materials

Aluminium (Alpoco, 99.7% pure, $D_{50} = 38 \mu\text{m}$), silicon (Wacker Chemie, 99.5% pure, $D_{50} = 26 \mu\text{m}$), copper (Chempur, 99.5% pure, $D_{50} = 27 \mu\text{m}$) and zinc (Grillo Werke, 99.99% pure, $D_{50} = 126 \mu\text{m}$) metal powders and powdered TiH_2 serving as blowing agent (Chemetall, Grade N, 98.8% pure, $D_{50} = 14 \mu\text{m}$) were used to prepare foamable precursors. Two different types of TiH_2 were used – as-received and heat-treated at $480 \text{ }^\circ\text{C}$ for 180 min under air. This treatment shifts the hydrogen release range to higher temperatures, which is essential for Al alloys [1]. To prepare Al-based precursors, 30 g of metal powder(s) were mixed with 0.5 wt.% of heat-treated TiH_2 powder in a tumbling mixer for 15 min. The powder blend was subjected to uni-axial hot compaction for 5 min at $400 \text{ }^\circ\text{C}$ applying a pressure of 300 MPa. For zinc, 80 g of powder and 0.6 wt.% of as-received TiH_2 were used and the compaction temperature was reduced to $350 \text{ }^\circ\text{C}$. Some precursor materials were prepared in the same way, but without the addition of TiH_2 . Cylindrical tablets (36 mm diameter, ~11 mm thickness) were obtained. $10 \times 10 \times 4 \text{ mm}^3$ large samples were cut out from these tablets, ensuring that the compaction direction was along the 4 mm long side of the sample (defining the foaming direction). The alloys used are listed in **Table 1**. AlSi6Cu4 and AlSi7 were the main alloys used in this study and only a few exploratory experiments were performed for pure Al, AlSi11 and Zn.

2.2. Foaming furnaces

Foaming was carried out in X-ray transparent furnaces. Two different furnaces were used. In the *lamp furnace*, two or three (for pure Al) halogen lamps of each 150 W power were used in conjunction with an infrared reflector [13]. Foaming was performed

inside a steel tube ($25.5 \times 25.5 \text{ mm}^2$ cross section, 2 mm wall thickness) that was 28 mm long and oriented in the direction of the X-rays. The open ends of the tube were covered with aluminium foils (thickness 0.03 mm) to minimize heat losses by convection during foaming. The steel tube was placed on a ceramic plate to further minimize heat losses. A thermocouple was inserted 0.5 mm deep into the foam from below through a hole in the steel tube. All samples containing TiH_2 were foamed in air using this lamp furnace.

TiH_2 -free samples were foamed by gas pressure manipulation [3] in a gas-tight *pressure furnace* that allows for foaming under controlled pressure and gas atmosphere. This furnace had a stainless steel casing and aluminium windows for the X-ray beam to pass through. The ceramic heating plate on which the samples were foamed had a maximum heating power of 600 W. The sample temperature was measured by a thermocouple which was led through the heating plate and protruded 0.5 mm into the foaming sample from below.

2.3. Experimental procedure

Samples containing blowing agent were foamed by heating them to above their melting point. In the lamp furnace the foaming temperature was 600 °C for all the Al alloys and 660 °C or 430 °C for pure Al or Zn, respectively.

Inserting a thermocouple far enough into the small specimens to ensure a reliable temperature measurement not only affected the stability and expansion of the foams but also disturbed the X-ray images. Therefore, the temperature was measured near the bottom surface, just 0.5 mm inside each sample. Due to the influence of the steel tube, the *surface* temperature T_s measured here deviated from the true sample temperature T_i . In order to determine this true *interior* temperature T_i , some calibration

experiments were carried out using two thermocouples – one at the bottom surface and another inside the sample. It was observed that at the foaming temperature (i.e., $T_s = 600\text{ °C}$) T_i was about 20 °C higher than T_s throughout the foaming experiment and sudden changes in T_i appeared smoothed out in the reading of T_s . Unless otherwise indicated, all the temperatures reported in this article correspond to T_s .

To standardize nomenclature, heating from room temperature ($\sim 30\text{ °C}$) up to the foaming temperature is considered as *heating stage*. The heating rate ranged from 2–3 K/s. The next stage, where temperature remained at or slightly above the foaming temperature, is denoted as holding stage and the corresponding time spent there is the *holding time* (HT). Because of temperature fluctuations, the maximum temperature reached during holding was $\sim 605\text{ °C}$ for a set point of 600 °C . After holding, the foam was allowed to cool down. 0 s holding time indicates that cooling started immediately after the temperature reached the set point. While *ambient cooling* was done by simply turning off the power supply of the lamps, *slow cooling* was achieved by decreasing the power of the heating lamps to a lower value.

To foam blowing agent-free samples, the powder compacts were first heated up to the foaming temperature inside the pressure furnace in an argon atmosphere pressurised to 5 bar. After melting of the samples, the gas pressure was released to 1 bar ambient pressure within 30 seconds. The pressure drop immediately induced expansion of the sample driven by the release of adsorbed gases present in the powder compact [3]. After pressure release, the experiments were identical to those of the samples containing blowing agent. As described for the lamp furnace, the thermocouple in this furnace is also influenced by the heating plate. Therefore, prior to performing the actual experiments, the temperature set point was determined such that the temperature inside

the sample ranged from 620 to 630 °C during foaming, which is above the melting point of the AlSi6Cu4 alloy used.

Foaming was continuously monitored *in-situ* by using an X-ray radiography set-up comprising a micro-focus X-ray source and a panel detector, see Ref. [13]. In this work, the X-ray source had 5 µm spot size and was operated at 100 kV voltage and 100 µA current. Series of X-ray projected images of the foam were obtained and analysed with the dedicated software ‘AXIM’ [18]. Expansion was expressed in terms of the growth of the projected area of the sample.

3. Results

3.1. Foaming stages

Fig. 1(a) shows the area expansion and temperature profile for alloy AlSi6Cu4 + 0.5 wt.% TiH₂, applying 100 s HT and solidifying by natural cooling. **Fig. 1(b)** represents the same data as a function of temperature. The three stages of foaming — namely heating, holding and cooling — can be directly correlated with features of the temperature course. Other alloys behave in a similar way.

3.2. Expansion during solidification

An intermediate expansion stage after a period of cooling followed by further shrinkage is indicated by arrows in both graphs of **Fig. 1**. The region marked by a broken box in **Fig. 1(a)** is enlarged in **Fig. 2**. There, point 1 indicates the onset of cooling, after which the foam still continues to expand until after a few seconds shrinkage begins. At point 2 the rate of shrinkage slightly decreases. This not very prominent feature is observed in all the measurements. After a local minimum at point 3

($A_{\min,1}$) the foam starts to expand up to point 6 ($A_{\max,2}$), followed by shrinkage for the remaining cooling process. As the intermediate expansion occurs during solidification of the foam, the term *solidification expansion* (SE) was coined. The total SE is given by the difference of the area expansion values in points 6 and 3. In **Fig. 2**, SE is 5.4% of the initial precursor area. SE is not totally uniform, but shows kinks at points 4 and 5 and hence can be divided into two stages – the first from point 3 ($A_{\min,1}$) to 4 ($A_{\max,1}$) and the second from point 5 ($A_{\min,2}$) to 6 ($A_{\max,2}$). This leads us to the definition of two partial expansions:

$$SE1 = (A_{\max,1} - A_{\min,1}) \quad (1)$$

$$SE2 = (A_{\max,2} - A_{\min,2}) \quad (2)$$

3.3. Cooling rate curve and SE

In **Fig. 2**, the first derivative of T_s (i.e., $\Delta T_s/\Delta t$) is displayed along with the area expansion data. Three temperature arrest peaks due to the release of latent heat during phase transformations are visible, corresponding to primary Al, binary Al-Si and Al-Si-Cu ternary phase solidification, respectively [19]. The interesting points on both curves are indicated. Cooling of the foam effectively starts at point 7, reflected by an increase in cooling rate. The first minimum (point 8) of the cooling rate curve is followed by a change in slope in the expansion curve (point 2). SE1 (point 3 to 4) is located approximately in between the first (point 8) and second (point 9) minima, whereas SE2 (point 5 to 6) is situated in between the second (point 9) and third (point 10) minima.

The corresponding temperatures of the interesting points in Fig. 2 can be extracted from the respective temperature (T_s) curve. For AlSi6Cu4 this was done for points 2 – 6 and 8 – 10 applying 0 to 3000 s HT and natural cooling, see **Fig. 3**. Each

data point represents the average of 3 to 7 experiments, except the data points for 50, 150, 250, 350, 450, 2000 and 3000 s HT that represent just a single measurement. The measurements for 50, 150, 250, 350 and 450 s HT, representing a second set of experiments, show a systematic temperature offset compared to the other points, thus underlining the difficulty of determining the temperature of expanding foams.

Fig. 3 demonstrates that the first minimum (point 8) is closely followed by the change of slope (point 2) in the expansion curve. Similarly, point 5 follows 9 and 10 follows 6 to a lesser extent. SE1 is situated in between the first and second minima, whereas SE2 appears in between the second and third minima. The differences between the SE1 start and end temperatures are smaller for short HTs, whereas the differences between the SE2 start and end temperatures appear nearly constant for all HTs.

3.4. Effect of HT on SE

The values of SE1 and SE2 for AlSi6Cu4 are shown in **Fig. 4(a)** for 0 to 3000 s HT. The error bars represent standard deviations. SE1 increases rapidly up to 200 s HT, after which it appears nearly constant within the error limits. SE1 then decreases after 450 s HT and no SE1 can be found for a HT longer than 500 s. On the other hand, SE2 is present for all HTs. It increases from 0 to ≈ 150 s HT and then gradually levels off to a constant value of $\approx 1.5\%$ that is reached after 600 seconds. As it was observed that the time period during which SE occurs varies among the experiments, time-normalised SE values, i.e. the rates of SE, are given in the inset of **Fig. 4(a)**. Before normalization, an estimate for gas precipitation in the SE temperature interval was subtracted while estimates for gas shrinkage and solidification shrinkage were added to isolate the effect caused by TiH₂. All time-normalized SEs in this article were calculated this way, the

details of which are given in section 4.5. The normalized SE shows a trend similar to that of the total SE.

AlSi7 also exhibits two stages of SE. SE1 and SE2 and their time-normalised values for three different HTs are given in **Fig. 4(b)**. SEs and normalised SEs are similar in trend and show the same behaviour found for AlSi6Cu4.

3.5. Effect of cooling rate on SE

It was observed that at cooling rates slower than the natural one SE1 increases significantly, while the variation in SE2 was insignificant. This is why the dependence on cooling rate is presented only for SE1.

The cooling part of the area expansion of three slowly cooled AlSi6Cu4 foams is shown in **Fig. 5(a)**. Although in all cases cooling was performed by reducing the power of the lamps from 300 to 180 W, a slight variation in cooling rate was measured. All the cooling rates mentioned in **Figs. 5** and **6** correspond to the average cooling rate, calculated simply by dividing ΔT by Δt during SE1. The values of SE1 given in **Fig. 5(a)** – 25 to 35% – are much larger than those obtained during natural cooling where SE is in the order of just 4.5% , see **Fig. 4(a)**. In **Fig. 5(a)**, the absolute expansion of each foam at the end of SE1 is higher than the peak expansion before cooling.

The rate of area expansion (dA/dt) during cooling is displayed in **Fig. 5(b)**. During cooling, dA/dt initially decreases up to point a, after which dA/dt increases to a maximum value at some instant during SE1. The positive part of dA/dt in **Fig. 5(b)** signifies SE1. It was observed that the reversal in the dA/dt value at point a coincides with the beginning of primary Al solidification. The fluctuation in the dA/dt curve is a result of disturbances caused, e.g., by cell wall ruptures.

SE1 and their respective time-normalized values for AlSi6Cu4 foam cooled at three different rates are compared in **Fig. 6(a)**. SE1 decreases with increasing cooling rate for each HT. In contrast, the time-normalized SE1 exhibits a slight increase with cooling rate.

SE1 and their respective time-normalized values (inset) in AlSi7 foams cooled at seven different cooling rates are displayed in **Fig. 6(b)**. For the given experimental parameters HT and cooling rate, SE1 is higher in AlSi7 than in AlSi6Cu4, compare **Figs. 4(a)** and **4(b)**. This was the reason to concentrate on AlSi7 for the cooling rate study. Each data point in **Fig. 6(b)** is the average of at least 3 measurements, except the one for 1.28 K/s that represents natural cooling. From 0.4 to 0.48 K/s a sharp decrease in SE1 is observed, after which SE1 drops almost linearly with the exception of the last point. Alike AlSi6Cu4, the time-normalized data for AlSi7 also increases as cooling rate increases.

3.6. SE in the other alloys

In AlSi11 alloy foamed applying 0 s HT and natural cooling, SE1 and SE2 are 1.3% and 3.2%, respectively. For all longer HTs, AlSi11 does not show any SE. When cooling this alloy at a slower rate, it was observed that instead of shrinking it kept on expanding for a long time for all applied HTs up to 500 s. For example, the sample foamed after 0 s HT and then cooled with an average cooling rate of 0.16 K/s, kept on expanding for 350 s. After the onset of shrinkage no SE was observed.

In pure aluminium, SE was not observed either during natural or during slow cooling. In contrast, a pure Zn sample exhibited one SE stage for both natural and slow

cooling, typical values being 5.9% for 50 s HT at 1 K/s cooling rate and 10.3% for 100 s HT at 0.62 K/s cooling rate. All these findings are summarised in **Table 1**.

3.7. SE in TiH₂-free samples

SE was also observed in samples foamed without using TiH₂. A typical example of the evolution of AlSi₆Cu₄ foam expanded by pressure manipulation only is shown in **Fig. 7**. During heating, the pressure increased slightly due to the temperature increase in the closed chamber and finally reached about 5.5 bar. After 100 s at the foaming temperature, the pressure was reduced to 1 bar, which immediately induced foaming. After 500 s HT at 1 bar, natural cooling was initiated. The cooling part shows one SE, an enlarged view of which is given in the inset. A change in slope during the initial part of cooling can be seen; this is equivalent to point 2 in **Fig. 2**. SE in this case is 2.2%. The cooling rate during SE is about 3 K/s. At a slower cooling rate, SE seems to have larger values. However, in TiH₂ free samples SE is very small and the effect of cooling rate could not be determined with sufficient accuracy.

4. Discussion

4.1. Possible volume loss and gain mechanisms

The mechanisms that could possibly increase or decrease the volume of a metal foam during solidification are listed in **Table 2**. Of the seven possible mechanisms, five that are thought to be relevant for real metal foams will be discussed in the next section, two are considered irrelevant, namely recalescence and rupture.

During solidification of pure alloys, *recalescence* (i.e., a temperature increase after undercooling [20]) could increase both the volume of the gas inside the bubbles

and stimulate gas production by the blowing agent. As the alloys investigated in this study contain a lot of oxides [11], strong heterogeneous nucleation at undercooling temperatures below 1 K [20] is expected, and therefore the corresponding recalescence effect is too small to cause SE.

Rupture of outer surface bubbles causes a sudden drop in volume. During solidification at natural cooling conditions, no significant outer surface rupture was observed. Only in few cases such rupture events during slow cooling have been recorded, see **Fig. 5(a)** for an example, but this effect is too rare to explain SE.

The total volume change during solidification is a combination of all the *volume gain* (VG) and *volume loss* (VL) mechanisms:

$$\frac{\partial V}{\partial t} = \frac{\partial V_{VG}}{\partial t} - \frac{\partial V_{VL}}{\partial t}, \quad (3)$$

where V_{VG} and V_{VL} represent the volumes (expressed as absolute values) contributed by the volume gain and loss mechanisms, respectively. Whenever $\partial V_{VL}/\partial t > \partial V_{VG}/\partial t$, shrinkage occurs, whereas $\partial V_{VG}/\partial t > \partial V_{VL}/\partial t$ implies foam expansion. In terms of the volume gain and loss mechanisms listed in **Table 2**, Eq. 3 can be expressed as

$$\frac{\partial V}{\partial t} = \frac{\partial}{\partial t} (V_{HP} + V_{HPr} - V_{SS} - V_{GS} - V_{HD}), \quad (4)$$

where V_{HP} represents the volume contributed by *hydrogen production* (HP) from the TiH_2 and V_{HPr} that caused by hydrogen precipitation. From these the volume losses by solidification shrinkage (SS), gas shrinkage (GS) and hydrogen out-diffusion (HD) are subtracted.

Note that the expansions given in this work represent projected area, not volume expansion. Due to surface tension, fully expanded foam appears nearly spherical [12].

To a good approximation, relative changes in projected area are therefore related to relative changes in volume, i.e., $A \approx (V)^{2/3}$.

4.2. Reason for SE – kinetic effects

Solidification shrinkage (SS) of the alloys used was either calculated using the commercial software package JMatPro [21] or taken from literature. For the commercial A319 casting alloy that resembles our AlSi6Cu4 alloy, SS is about 6%, its projected area counterpart is 4%. For AlSi7, AlSi11, Al and Zn, SS is about 6% [21], 5% [22], 7% [23] and 4% [23], respectively. Their corresponding projected area counterparts are 4%, 3.5%, 4.4% and 3%, respectively.

Shrinkage of the hydrogen gas (GS) inside the foam can be calculated by using the ideal gas law, $V \propto T$, where T is the absolute temperature. For the area shrinkage counterpart, $A \propto T^{2/3}$ holds.

The shrinkage of the gas present inside the foam should be estimated using the inside temperature T_i measured in the calibration experiment rather than using the surface temperature T_s measured in the actual foaming experiment since the reading of T_s is disturbed as discussed before. In **Fig. 8(a)**, the shrinkage for an AlSi6Cu4 foam calculated from the beginning of solidification is given. Note that the starting points of Al-Si binary and Al-Si-Cu ternary solidification visible in the T_i and T_s temperatures differ slightly by ≈ 5 s as expressed by the slanted broken lines in **Fig. 8(a)**, which has to be corrected.

Fig. 8(b) shows the derivative dA/dt of the projected foam area A during cooling. The solidification of primary Al and binary Al-Si phase coincides with the changes observed in the dA/dt curve at the points a and b, respectively. This is caused

by the latent heat produced during solidification of these phases which immediately slows down both the temperature decrease and the shrinkage of the foam. Solidification of the ternary phase does not cause any notable change. **Fig. 8(b)** shows that dA/dt reaches a peak between points 3' and 4', which is a similar behaviour as seen in **Fig. 5(b)**. The fluctuations are caused by cell wall rupture.

Of the 279% area expansion at the start of solidification in **Fig. 8a**, about 6% are due to the expansion of the metallic phase, so that the reference value for the gas volume is 273%.

During solidification of primary Al, the cooling rate decreases temporarily, resulting in a very flat region of the calculated expansion curve in the early stage of solidification, see **Fig. 8(a)**. In the measured expansion curve this is reflected by a change in slope (point 2). Up to point 3, the measured data show far more shrinkage than gas shrinkage alone would suggest. This large difference is caused by continuous gas losses due to *out-diffusion of hydrogen* that overcompensates H_2 production since SS cannot produce such a large effect. From point 3 to 4, SE1 is observed, suggesting $\partial V_{HD}/\partial t < \partial V_{HP}/\partial t$ here. This reduction of gas loss rate that takes place in a small temperature interval ($\Delta T \approx 18$ K) while the other expansion-controlling factors are virtually unchanged is the key feature of SE. Analysis of the dA/dt curve in **Fig. 8(b)** suggests that the reduction in gas loss rate is actually initiated at the onset of primary Al solidification (point a), long before SE1 starts. This implies that the reduction of gas loss is intimately connected with the solidification of primary Al.

When foaming is performed in the presence of oxygen, an oxide layer forms on the outer surface as illustrated in **Fig. 9(a)** [24]. Under isothermal conditions, the rate of gas diffusing out of liquid aluminium foam is largely controlled by this oxide layer

[12,24]. The oxide layers also influence gas loss during solidification. Therefore, in the following we estimate gas loss during solidification considering both the solidification of primary Al and the formation of oxide layers.

In equilibrium, the flux of hydrogen through the liquid Al layer is equal to that through the oxide layer. This can be written for the case shown in **Fig. 9(a)** as [24]

$$D_{H \rightarrow Al-L} \cdot \frac{C - C_1}{d_{Al-L}} = D_{H \rightarrow Al_2O_3} \cdot \frac{C_1}{d_{Al_2O_3}} \quad (5)$$

$D_{H \rightarrow Al-L}$ and $D_{H \rightarrow Al_2O_3}$ are the diffusion coefficients of hydrogen in liquid Al and Al_2O_3 , respectively and d_{Al-L} and $d_{Al_2O_3}$ are the corresponding thicknesses. C is the hydrogen solubility in liquid Al at 660 °C which is $\approx 0.05 \text{ cm}^3/\text{cm}^3$ of Al [24,25]. The interfacial concentration C_1 must be less than or equal to the hydrogen solubility in Al_2O_3 , the effective value of which at 660 °C is $\approx 0.05 \text{ cm}^3/\text{cm}^3$ of Al_2O_3 , accidentally the same as in liquid Al [24,26]. According to Eq. 5, the flux J through either of the layers is:

$$J = \frac{D_{H \rightarrow Al-L} \cdot D_{H \rightarrow Al_2O_3}}{d_{Al-L} \cdot D_{H \rightarrow Al_2O_3} + d_{Al_2O_3} \cdot D_{H \rightarrow Al-L}} \cdot C \quad (6)$$

The influence of various factors on gas loss is illustrated in **Fig. 10** where in consecutive steps additional parameters governing diffusion are included.

Firstly, diffusion slows down as temperature drops. For the calculation, the thicknesses $d_{Al-L} = 100 \text{ }\mu\text{m}$ and $d_{Al_2O_3} = 36 \text{ nm}$ were taken from Ref. [24], and for the diffusion coefficients as a function of T , $D_{H \rightarrow Al-L} = 3.8 \times 10^{-2} \times \exp(-4600/1.987T) \text{ cm}^2/\text{s}$ [27], and $D_{H \rightarrow Al_2O_3} = 9.7 \times 10^{-4} \times \exp(-79990/8.314T) \text{ cm}^2/\text{s}$ [28] were used. The radius of the spherical foam is 7 mm [12] with an area expansion at the start of solidification as read from **Fig. 8(a)**. The calculation shown in **Fig. 10** covers the

temperature (T_i) range of primary Al solidification in **Fig. 8(a)**. In the relevant temperature interval, the diffusion coefficient and consequently the volume loss rate (dV_{HD}/dt) decrease. This is shown by line A in **Fig. 10**. The change in dV_{HD}/dt at the start of SE1 is $\approx -20\%$.

Secondly, $d_{Al_2O_3}$ increases during the 25 s of cooling. Since the sample has been held for 200 s at 600 °C prior to cooling, a further increase in oxide thickness should be no more than a few nanometres. The data provided in Ref. [29] suggest an approximately linear increase by 3 nm, leading to line B. The change in dV_{HD}/dt at the start of SE1 is $\approx -24\%$.

Third, during solidification the cell wall material turns into a mushy state as dendrites of primary Al start penetrating the liquid metal. Here freely floating dendrites are considered. The diffusion coefficient of hydrogen in this state can be approximated by that of the liquid multiplied by the liquid fraction since diffusion in the solid state is negligible [27]. The solid content at the end of primary Al solidification is $\approx 50\%$ [20]. If we assume a linear increase of the solid fraction with temperature drop, we obtain line C in **Fig. 10**, displaying a change in dV_{HD}/dt at the onset of SE1 of $\approx -41\%$.

Finally, we consider that Al dendrites nucleate at the outer surface oxide layer, and subsequently grow as the temperature drops. In this way, the outer surface is partially covered by a solid Al layer. Consequently, the effective surface area of diffusion reduces since the diffusion through solid Al is negligible. We assume a linear increase of surface coverage until the outer surface is fully covered by solid Al at the end of primary Al precipitation. This results in line D in **Fig. 10**.

Another scenario could be that at the onset of solidification a solid Al layer forms in between the liquid Al and Al_2O_3 layers, and covers the entire surface. The

thickness of the oxide layer increases with time. In analogy to Eq. 5, the equilibrium equation for the case of **Fig. 9(b)** is:

$$D_{H \rightarrow Al-L} \cdot \frac{C - C_2}{d_{Al-L}} = D_{H \rightarrow Al-S} \cdot \frac{C_3 - C_4}{d_{Al-S}} = D_{H \rightarrow Al_2O_3} \cdot \frac{C_4}{d_{Al_2O_3}}. \quad (7)$$

$D_{H \rightarrow Al-S}$ and d_{Al-S} are the diffusion co-efficient of hydrogen in solid Al and the thickness of the solid Al layer. $D_{H \rightarrow Al-S} = 1.1 \times 10^{-1} \times \exp(-9780/1.987T)$ cm²/s [27]. As there is a significant difference in hydrogen solubility between solid and liquid Al, the concentration C_2 drops to a very low value C_3 at the liquid-solid interface of Al which is why it is sufficient to consider only the combination of solid Al and Al₂O₃ layer. Accordingly, Eq. 6 can be modified by replacing the diffusion coefficient and thickness of liquid Al by the values of solid Al, and C by C_3 . C_3 is equal to the hydrogen solubility in solid Al, which at 300 K is ≈ 0.0369 cm³/100 g Al [25]. At 660 °C, this is about 0.003 cm³/cm³ of Al. The thickness of the solid Al layer we assume to grow linearly from 1 to 50 μm in the temperature range of **Fig. 10**, leading to line E. Obviously, the formation of a continuous solid Al layer immediately reduces out-diffusion drastically. Further solidification hardly causes any change in dV_{HD}/dt . Therefore, if a continuous solid Al skin was formed, this would have to happen when SE1 starts as indicated by the broken line connecting points c and e in **Fig. 10**.

A complete coverage by a solid Al layer at the onset of SE1 would result in an abrupt change in dA/dt . However, the course of dA/dt shown in **Fig. 8(b)** (and in **Fig. 5(b)**) suggests a continuous variation which is only possible if the gas loss follows either line C or line D, or a combination of both.

There are few limitations of the diffusion model employed here. The surface of a real foam is corrugated due to the presence of an oxide layer [30], and therefore the

effective surface area is always higher than the theoretical one. During shrinkage the oxide layer may break and provide an easy path for diffusion. The diffusion coefficient of hydrogen in pure Al is used since there is no data available for the alloys used in this work. We have addressed these limitations in a recent study [24], where it has been shown that despite some limitations, this diffusion model agrees well with measurements.

After the losses have been largely reduced, the volume gain by hydrogen still being released by the blowing agent dominates and thus results in SE1.

Hydrogen precipitation from the melt can also contribute to SE1, but since SE1 was observed only for shorter HT (up to 500 s), H₂ production from TiH₂ is definitely the main source of SE1.

After point 4, there is some further shrinkage up to point 5, which is caused by an increase in $\partial V_{GS}/\partial t$ due to a faster cooling towards the end of primary Al solidification. **Fig. 2** proves that the cooling rate increases towards the end of the solidification of each phase. Note that this behaviour in the intermediate region of points 4 and 5 is not always reproducible: foams may or may not shrink from point 4 to point 5 (for example, compare **Figs. 2** and **8**).

SE2 also requires production of gas to overcompensate losses. This gas comes both from TiH₂ and the dissolved gas present in the melt, the details of which will be given later. Beyond point 6 there is no significant shrinkage. The gas inside the foam can no longer follow the gas law due to the presence of a high amount of solid fraction (≈ 0.9 [20]) in the matrix generated during solidification.

Note that both foam expansion and contraction could be affected by the changing properties of the melt even in earlier stages of solidification, e.g. by its

changing viscosity or even shear-rate dependent properties of the semi-solid liquid, but a precise description of such effects is beyond the available models.

The outer surface oxide layer may cause mechanical resistance against stretching and therefore hinder further expansion [11,12,30]. Typically, AlSi6Cu4 foam will shrink by 10–15% from peak expansion to the start of SE1, during which the oxide films do not shrink but fold up to a wrinkly surface. Re-expansion during combined SE1 and SE2 under natural cooling conditions is below the level of prior shrinkage (see Figs. 1, 2, 7 and 8) and will simply unfold the oxides again without the need to stretch or break them. Just in special cases such as slow cooling SE is high enough to allow the oxides to exert significant forces, see section 4.5.

4.3. Effect of holding time on SE

Hydrogen production from TiH₂ can continue for a prolonged period, typically for more than an hour [1, 2]. In the present study, TiH₂ releases hydrogen even during the solidification of foams, the amount of which depends on HT. For short HTs, the rate of hydrogen production is so strong that the foam in Fig. 2 continues to expand even though cooling has started.

For a given alloy and cooling rate, $\partial V_{HP}/\partial t$, $\partial V_{SS}/\partial t$ and $\partial V_{GS}/\partial t$ in Eq. 4 are constant for all HTs. Therefore, the variation in SE with HT shown in Fig. 4(a) is attributed only to the change in $\partial V_{HP}/\partial t$ and $\partial V_{HD}/\partial t$ with holding time. With increasing HT, hydrogen production from TiH₂ decreases. According to the data provided by Ref. [1] for TiH₂-containing AlSi6Cu4 precursor, the hydrogen production during isothermal holding can be fitted by an empirical function as given in Fig. 11. On the side of gas losses, holding takes place in the liquid state and the only possible change of

the loss rate is by oxidation. The growth behaviour of the alumina layer was estimated from the data provided in Ref. [29] and the out-diffusion was calculated based on the flux obtained from Eq. 6, leading to another empirical function as given in **Fig. 11**. It can be shown that the combination of hydrogen production and out-diffusion results in a peak in the SE as qualitatively illustrated in **Fig. 11**.

Since $\partial V_{HD}/\partial t$ is larger for a shorter HT (due to a thinner oxide film), SE1 starts at a later stage during solidification. $\partial V_{HD}/\partial t$ decreases with increasing HT because the oxide layer becomes thicker. For longer HT, the gas loss can therefore be compensated in an earlier stage. This is why the onset of SE1 shifts towards higher temperature with increasing holding time, see point 3 in **Fig. 3**. For the same reason, SE1 is the smallest for 0 s HT and increases with HT as shown in **Fig. 4(a)**. $\partial V_{HP}/\partial t$ and $\partial V_{HD}/\partial t$ act together in tandem and keep the SE1 value at nearly a constant level between 200 and 450 s HT, after which the decrease of $\partial V_{HP}/\partial t$ dominates and SE1 drops rapidly to a level where it can no longer be measured (after 500 s HT). AlSi7, see **Fig. 4(b)**, behaves in a similar way.

For SE2, the behaviour up to 600 s HT can also be explained by hydrogen production from the TiH_2 concomitant with gas loss. Unlike SE1, SE2 remains at a constant value after this, pointing at precipitation of hydrogen from the melt as the main reason, since this mechanism is constant and therefore does not depend on HT. Hydrogen precipitation is also present for 0 to 500 s HT; there it is superimposed with the HT-dependent effect of hydrogen evolution from TiH_2 .

4.4. Hydrogen precipitation

Precipitation of H₂ during solidification produces gas porosity in aluminium products [23,31]. The amount of precipitation from Al and some Al-Si alloys is given in **Fig. 12** based on data reported in Ref. [25]. In addition, hydrogen solubilities were calculated using Wagner's interaction parameters for 700 °C [32,33]. The solubility values quoted in the literature refer to the volume at 300 K. When precipitated gas leads to formation of pores, one has to consider the corresponding volume at the precipitation temperature T_{prec} , which is $T_{\text{prec}}/300\text{K}$ times higher [12].

The volume fraction of gas precipitated at the liquidus temperature (T_L) and the gas solubilities (calculated using Wagner's interaction parameters) at 700 °C are given in **Table 3** as actual volume fractions at that temperature. H₂ precipitation at T_L of AlSi7 is about 50% of the calculated value at 700 °C. Since AlSi7 and AlSi6Cu4 have similar T_L , 615 and 610 °C respectively, about 2.5 vol.% of H₂ precipitation is expected for AlSi6Cu4 at its T_L [12]. This amount corresponds to 1.5% (area) SE2 in this alloy. The precipitation of hydrogen is diffusion-controlled and therefore depends on the kinetics of solidification. Ideally, for very slow cooling, precipitation should immediately follow solidification. In contrast, for natural cooling, it is shifted towards lower temperature. In the present study, it appears that most of the precipitation takes place during binary Al-Si phase solidification, where it results in SE2.

Hydrogen precipitation is a property of the alloy, and therefore, it is independent of the presence of TiH₂. When TiH₂-free samples are melted and foamed by pressure variation, the reaction between metal and adsorbants present in the metal powder produces some hydrogen which is then dissolved in the melt [3]. Subsequent solidification leads to precipitation of this hydrogen and results in SE as observed in the TiH₂-free AlSi6Cu4 foam in see **Fig. 7**.

In AlSi6Cu4, the solidification shrinkage (SS) during binary Al-Si phase solidification is about 2 vol.% [21], a part of which (≈ 1.2 vol.%) occurs during SE2 since it covers $\approx 60\%$ of this solidification temperature interval as shown in Fig. 3. Therefore, if the amount of H₂ precipitation is more than 1.2 vol.% it can produce SE after compensating SS. Except for a eutectic composition, multi-component alloys show pasty solidification [23]. Because of this, SS is mainly manifested as shrinkage porosity in AlSi6Cu4 foam [12], and thus it is not reflected effectively by a reduction of the overall projected area. As a result, H₂ precipitation produces SE without having to fully compensate SS. It is difficult to predict how much hydrogen will be absorbed by the shrinkage porosity but experimental evidence suggests that some will be available to produce SE. In contrast, since pure Al and near-eutectic AlSi11 are skin-freezing alloys, most part of their SS will be reflected in the area expansion curve. Therefore, although the amount of H₂ precipitation in Al is 5 vol.% (see Table 3), this is not sufficient to compensate for its 7% SS and therefore cannot produce SE. No SE2 was observed in AlSi11 for longer HT, where the same holds.

4.5. Effect of cooling rate on SE1

For a given HT and alloy, SE can be expressed as:

$$SE = \int_0^{t_{SE}} \frac{\partial}{\partial t} (V_{HP} - V_{HD}) dt + \int_{T_0}^{T_{SE}} \frac{\partial}{\partial T} (V_{HP} - V_{GS} - V_{SS}) dT, \quad (8)$$

where, $(0, t_{SE})$ and (T_0, T_{SE}) are the time and temperature interval of SE, respectively. The first term on the *rhs* of Eq. 8 depends on the cooling rate, while the second term depends on the temperature interval only. Rearrangement of Eq. 8 yields

$$SE - (V_{HP} - V_{GS} - V_{SS}) \Big|_{T_0}^{T_{SE}} = \int_0^{t_{SE}} \frac{\partial}{\partial t} (V_{HP} - V_{HD}) dt = \int_0^{t_{SE}} R(t) dt \quad . \quad (9)$$

Now the *rhs* of Eq. 9 represents the part of SE resulting only from the balance of hydrogen production from TiH₂ and out-diffusion of hydrogen. When the cooling rate decreases, the time period of SE increases. This leads to a larger value of the *rhs* of Eq. 9. Since the temperature range of SE at different cooling rates does not vary significantly, the integration product on the *lhs* of Eq. 9 is nearly the same for all the cooling rates studied here. Hence, the increase in t_{SE} is the main reason for larger SE1 at lower cooling rates as shown in **Figs. 5** and **6**.

Fig. 5(a) shows that the expansion achieved at the end of SE1 is higher than the peak expansion of the foam. The same is true for AlSi7 foams for all the cooling rates applied in this study. When a foam regains its peak expansion during SE1, it needs more internal pressure in order to expand further. This is to counteract the mechanical resistance imposed by the cell walls and the surface oxide layer. It is not completely clear whether the internal pressure increases even before regaining peak expansion, but it is expected to increase after reaching peak expansion. In **Fig. 5(b)**, the decrease in dA/dt after reaching a maximum is because of the combined effect of increasing mechanical resistance and decreasing hydrogen production. The trend in the dA/dt curve for the other foams shown in **Fig. 5(a)** is similar (see supplementary online material **A**).

Note that in Eq. 9 there is no explicit parameter which accounts for the mechanical resistance discussed above. $\partial V_{HP}/\partial t$ automatically includes this resistance since part of the hydrogen production is used for increasing the internal pressure of the foam. If foam consisted of only the outer surface, the mechanical resistance could be estimated as demonstrated in Refs. **11** and **12**. But foam is a complex structure

containing many cells where the stresses are shared among all the cell walls and Plateau borders. When it comes to individual cells, the internal expansion during SE becomes even more complex. It is seen that SE is not the same everywhere inside a foam (see supplementary online material **B**) [12,16]. This implies that the resistance against expansion varies significantly from one cell to another. However, the estimation of the mechanical resistance during expansion is difficult and beyond the scope of this work.

A cooling rate-independent R in Eq. 9 would imply that SE1 is proportional to the time needed for solidification. We divide the *lhs* of Eq. 9 by t_{SE} and display the result as ‘time-normalized SE1’ in the insets of **Figs. 6(a)** and **6(b)**. This value would simply be R/t_{SE} . The small slope found actually expresses the slight increase in average gas production rate with increasing cooling rate.

The time-normalized SEs in the insets of **Fig. 4** were calculated in the same way. For different HTs they all follow the same trend as the non-normalized SEs. This demonstrates that the effect of HT on SE is not related to the duration of SE.

4.6. Effect of alloy composition on SE

Alloy composition has manifold effects on SE, some of which have already been discussed. For a given cooling rate and HT, the difference in melting point between different alloys affects the amount of remaining hydrogen in TiH_2 . A constant foaming temperature is used for all the alloys. The dissociation rate of TiH_2 is higher in the semi-solid or liquid than in the solid state of an alloy because the released hydrogen diffuses through the liquid much quicker than through the solid. For given experimental parameters, the time spent in the semi-solid and liquid state depends on the alloy composition. Dissociation is maximal in AlSi11 because it spends the longest time

(corresponding to $\Delta T = 35$ K) in the liquid state. This leads to a small amount of hydrogen available for SE. Therefore, except for 0 s HT, no SE was observed in AlSi11 samples. When AlSi6Cu4 and AlSi7 alloys are compared, both have similar liquidus temperatures, 610 and 615 °C, but a different semi-solid co-existence range, 85 K and 38 K for AlSi6Cu4 and AlSi7, respectively. Hence, the discharge of TiH₂ is more pronounced in AlSi6Cu4 than in AlSi7. Consequently, SE is higher in AlSi7 than in AlSi6Cu4 under identical conditions as shown in **Figs. 4(a)** and **4(b)**. The foaming temperature of pure zinc was 430 °C (m.p. 420 °C), while that for pure Al sample was 670 °C (m.p. 660 °C). As a consequence, the amount of remaining hydrogen is higher in Zn compared to Al. Moreover, solidification shrinkage in Zn is just 4 vol.%, compared to 7 vol.% in Al. For these reasons, SE was observed in zinc but not in aluminium.

Alloy composition influences the thickness of the oxide layers [23]. Since the oxide layer plays an important role in SE by controlling both gas losses and mechanical resistance, an alloy-dependent oxide thickness should also be taken into account for the sake of a complete description of SE.

A complete quantitative description of SE is still lacking. This is because the data necessary are not yet known, for example, the diffusion coefficient of hydrogen and the oxide thicknesses for the Al alloys used in this study, the dissociation behaviour of TiH₂ at falling temperature, the viscosity of the melt inside cell walls during solidification, etc. Nevertheless, based on the available data, the behaviour of SE and the mechanisms responsible for SE can be satisfactorily explained.

5. Conclusions

The study of metal foam solidification showed that

- 1) an expansion stage (*solidification expansion* or SE) was observed during solidification of many different types of metal foams. It can be partitioned into two contributions – SE1 and SE2 – in many cases,
- 2) SE1 is mainly a result of the interplay between gas shrinkage and gas losses due to out-diffusion on one hand, and ongoing H₂ production from the TiH₂ and H₂ precipitation during solidification on the other,
- 3) SE1 and SE2 are linked with the phase transformations during solidification,
- 4) SE occurs when the gas loss rate is reduced, while gas production remains nearly constant. The losses are reduced owing to the progressing solidification in the cell wall and a growing oxide layer,
- 5) SE depends on the holding time before cooling and shows a maximum value for 200 – 400 s HT,
- 6) SE1 vanishes for more than 500 s of holding. In this case, the reduced gas supply from the blowing agent can no longer overcompensate gas losses,
- 7) SE2 is present for all HTs and nearly constant for more than 500 s HT, pointing at precipitation of H₂ during solidification as reason for SE2,
- 8) the amount of SE2 is determined by the composition of the alloy and is independent of the presence of TiH₂, which is why SE was also observed in samples foamed without a blowing agent,
- 9) SE1 is larger for slower cooling as the alloy then spends more time in the regime where volume gain dominates gas losses,
- 10) the composition of alloy also influences SE because the regime of SE is shifted to different temperatures, which influences the kinetics of gas generation from TiH₂.

Acknowledgements – The authors would like to thank G.S. Vinod Kumar and Catalina Jiménez for their valuable suggestions.

References

- [1] Matijasevic-Lux B, Banhart J, Fiechter S, Görke O, Wanderka N. *Acta Mater* 2006;54:1887.
- [2] von Zeppelin F, Hirscher M, Stanzick H, Banhart J. *Comp Sci Tech* 2003;63:2293.
- [3] Garcia-Moreno F, Banhart J. *Coll Surf A* 2007;309:264.
- [4] Helfen L, Baumbach T, Pernot P, Cloetens P, Stanzick H, Schladitz K, Banhart J. *Appl Phys Lett* 2005;86:231907-1.
- [5] Banhart J, Stanzick H, Helfen L, Baumbach T. *Appl Phys Lett* 2001;78:1152.
- [6] Kennedy AR. *J Mater Sci Lett* 2002;21:1555.
- [7] Babcsan N, Garcia-Moreno F, Banhart J. *Coll Surf A* 2007;309:254.
- [8] Stanzick H, Wichmann M, Weise J, Helfen L, Baumbach T, Banhart J. *Adv Eng Mater* 2002;4:814.
- [9] Garcia-Moreno F, Rack A, Helfen L, Baumbach T, Zabler S, Babcsan N, Banhart J, Martin T, Ponchut C, Di Michiel M. *Appl Phys Lett* 2008;92:134104-1.
- [10] Körner C, Arnold M, Singer RF. *Mater Sci Eng A* 2005;396:28.
- [11] Dudka A, Garcia-Moreno F, Wanderka N, Banhart J. *Acta Mater* 2008;56:3990.
- [12] Mukherjee M. Thesis, Technische Universität Berlin; 2009.
- [13] Garcia-Moreno F, Babcsan N, Banhart J. *Coll Surf A* 2005;263:290.
- [14] Wu ZJ, He DP. In: Banhart J, Ashby MF, Fleck NA, editors. *Cellular Metals and Metal Foaming Technology*, Bremen: Verlag MIT Publishing, 2001. p.123.
- [15] Cox SJ, Bradley G, Weaire D. *Eur Phys J App Phys* 2001;14:87.
- [16] Mukherjee M, Garcia-Moreno F, Banhart J. *Scripta Mater* 2010;63:235.
- [17] Mukherjee M, Garcia-Moreno F, Banhart J. *Trans Indian Inst Met* 2007;60:133.
- [18] Garcia-Moreno F, Fromme M, Banhart J. *Adv Eng Mater* 2004;6:416.

- [19] Shabestari SG, Malekan M. *Cana Met Quart* 2005;44:305.
- [20] Backerud L, Chai G, Tamminen J. *Solidification characteristics of aluminum alloys*, vol. 2, Foundry Alloys. U.S.A.: AFS / SkanAluminium, 1990.
- [21] Thermotech Ltd. JMatPro - Materials property simulation package. <<http://www.thermotech.co.uk/>>.
- [22] Magnusson T, Arnberg L. *Met Mater Trans A* 2001;32:2605.
- [23] Campbell J. *Castings: the new metallurgy of cast metals*. second edition. Oxford: Butterworth-Heinemann, 2003.
- [24] Mukherjee M, Garcia-Moreno F, Banhart J. *Met Mater Trans B*; doi: 10.1007/s11663-010-9357-5.
- [25] Lutze P, Ruge J. *Metallwissenschaft und Technik* 1990;44:741.
- [26] Roy SK, Coble RL. *J Am Ceram Soc* 1967;50:435.
- [27] Eichenauer W, Markopoulos J. *Z Metallkde* 1974;65:649.
- [28] Serra E, Bini AC, Cosoli G, Pilloni L. *J Am Ceram Soc* 2005;88:15.
- [29] Freti S, Bornand J-D, Buxmann K. *Light Metals* 1982;1003.
- [30] Simancik F, Behulova K, Bors L. In: Banhart J, Ashby MF, Fleck NA, editors. *Cellular Metals and Metal Foaming Technology*, Bremen: Verlag MIT Publishing, 2001. p.89.
- [31] Mitrasinovic A, Robles Hernández FC, Djurdjevic M, Sokolowski JH. *Mater Sci Eng A* 2006;428:41.
- [32] Anyalebechi PN. *Scripta Met Mater* 1995;33:1209.
- [33] Anyalebechi PN. *Scripta Mater* 1996;34:513.

Figure captions

Figure 1. (a) Area expansion and temperature as a function of time for foaming of AlSi6Cu4 alloy. The temperature defines three stages of foaming – *heating*, *holding* and *cooling*. The holding time is 100 s followed by natural cooling. (b) Area expansion as a function of temperature for the same experiment as in (a). The cooling part of the area expansion curve in both (a) and (b) shows an expansion stage (SE), the beginning of which is indicated by an arrow. The broken box marks the area enlarged in **Fig. 2**.

Figure 2. Enlarged view of the area marked by a broken box in **Fig. 1(a)**, and the corresponding temperature derivative ($\Delta T_s/\Delta t$) as a function of time. Two expansion stages (SE1 and SE2) are seen. Interesting points are labelled by numbers and are explained in the text.

Figure 3. AlSi6Cu4 alloy: Corresponding temperatures (T_s) of the points 2–6, 8–10 of **Fig. 2** for 0 to 3000 s HT. Except for 500 s HT, error bars are avoided for the sake of clarity as they are in the same range for all HTs. The lines represent linear fits. Lines corresponding to each set of data are marked with the same number as in the legend of that data set.

Figure 4. SE1 and SE2 as a function of holding time for (a) AlSi6Cu4 and (b) AlSi7 alloy. All the experiments were performed with natural cooling. Average cooling rates during SE1 and SE2 are ~ 1.3 – 1.4 and 1.1 K/s, respectively. The inset shows the time-normalized SE as a function of holding time for each alloy. The error bars in (a)

represent the standard deviation. Each data point in (b) corresponds to a single measurement.

Figure 5. (a) Cooling part of the area expansion profile for AlSi6Cu4 foams that were foamed applying 200 s holding time and cooled slowly under the same conditions. The respective cooling rates are given in the legend. The value of SE1 for each cooling rate is given. (b) Area expansion and the corresponding rate of area expansion (dA/dt) of the foam cooled at 0.28 K/s. The maximum expansion reached before the foam starts to shrink is defined as peak expansion and is indicated by a solid arrow. The broken arrow indicates when the foam regains its peak expansion during SE1. The point a in the dA/dt curve indicates the time at which primary Al begins to solidify.

Figure 6. Effect of cooling rate on solidification expansion (SE1) and its time normalized value (inset). (a) For AlSi6Cu4, applying three holding times (HT). (b) For AlSi7, applying 100 s HT. The two rightmost points in (a) and the one rightmost point in (b) represent natural cooling. Error bars represent standard deviation in expansion and cooling rate, except where a single experiment is displayed or where the scatter is negligibly small.

Figure 7. Area expansion, foaming temperature and ambient pressure profile of a pressure induced foaming (PIF) experiment for AlSi6Cu4 alloy, SE is 2.2%. The temperature measurement is affected by the heating plate. A reading of 750 °C corresponds to a temperature of 620 °C to 630 °C inside the sample.

Figure 8. (a) Area expansion (legend “measured”) during solidification as a function of time of AlSi6Cu4 after 200 s of holding (natural cooling). Measured surface temperature T_s and interior temperature T_i (taken from a reference experiment), where the latter curve has been shifted such that aluminium precipitation begins at the same time for T_s and T_i . Calculated expansion (legend “simulated from start of Al precipitation”) based on the gas shrinkage using the temperature (T_i) inside the foam. The value of area expansion at the start of primary Al solidification is taken as the reference starting point of calculation. (b) Area expansion and the corresponding rate of area expansion (dA/dt) during cooling of the foam shown in (a). The corresponding time of the solidification of different phases are indicated by a–c in the dA/dt curve. The numbers 2–6 in (a) and (b) have the same significance as in **Fig. 2**. The corresponding points 3–6 of the area expansion curve are indicated by the points 3’–6’ in the dA/dt curve.

Figure 9. Illustration of the hydrogen flux and concentration gradient through the metallic and oxide part of a cell wall – (a) in liquid state, (b) after partial solidification. C and d represent concentration and thickness, respectively. Modified from Ref. **24**.

Figure 10. Volume loss rate through out-diffusion against time for five different combinations of liquid Al, solid Al and oxide layer. Line A: includes temperature dependence of diffusion coefficient only; Line B: includes also growth of oxide layer; Line C: includes also increasing solid fraction (mushy solidification); Line D: includes partial coverage of the outer surface by a solid Al layer (mushy solidification), Line E:

complete coverage of the outer surface by a solid Al layer (skin freezing). The details are discussed in the text.

Figure 11. Schematic representation of solidification expansion as a function of holding time HT in terms of hydrogen production from TiH_2 and out-diffusion of hydrogen. Parametrizations of the hydrogen production (HP) and out-diffusion (HD) are given, P_1 , P_2 and P_3 are parameters based on experimental data.

Figure 12. Hydrogen solubility in Al and Al-Si alloys at the liquidus temperature and above and below the solidus temperatures as a function of Si content. The straight lines are linear fits. Data extracted from Ref. [25](#).

Table 1

Occurrence of solidification expansion in different alloys, blowing agent usage and cooling conditions

Alloy	TiH ₂ used?	Solidification expansion found?		
			natural cooling	slow cooling
AlSi6Cu4	Yes	SE1	Yes	Yes
		SE2	Yes	Yes
	No	Yes, one SE	Yes, one SE	
AlSi7	Yes	SE1	Yes	Yes
		SE2	Yes	Yes
AlSi11	Yes	SE1	Yes	No
		SE2	Yes	
Al	Yes		No	No
Zn	Yes		Yes, one SE	Yes, one SE

Table 2

Possible mechanisms and their contribution to foam expansion during solidification

Effect on foam expansion	Mechanism
	Hydrogen production from TiH_2 (HP)
Volume gain (VG)	Precipitation of hydrogen from the metallic melt (HPr) Recalescence effects
	Solidification shrinkage of metallic matrix (SS)
Volume loss (VL)	Shrinkage of gas due to decreasing T (GS) Hydrogen out-diffusion or effusive losses (HD) Rupture of outer surface bubbles

Table 3

Effective volume of hydrogen precipitation (prec.) and solubility (sol.) in Al/Al-alloys assuming gas saturation in the melt with hydrogen. The volumes given are at the precipitation temperatures or at 700 °C

Alloy	Total (vol.%) H ₂ prec. at T_L , from Fig. 12	H ₂ sol. at 700 °C, (vol.%) [32,33]
Al	5	8
AlSi7	3.05	6.13
AlSi11	1.86	5.5
AlSi6Cu4	2.5 (estimated)	4.9

Figure 1(a)
[Click here to download high resolution image](#)

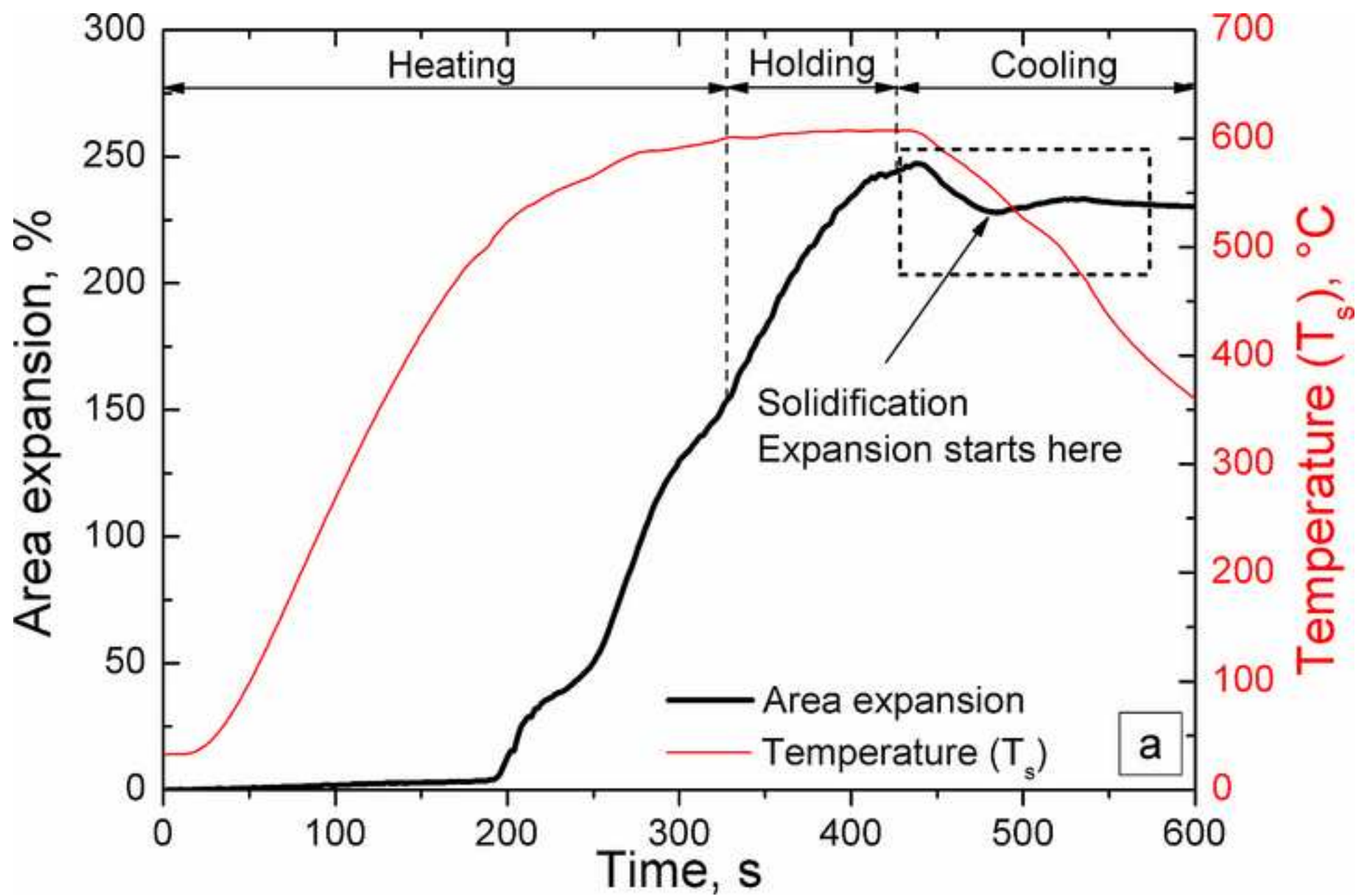


Figure 1(b)
[Click here to download high resolution image](#)

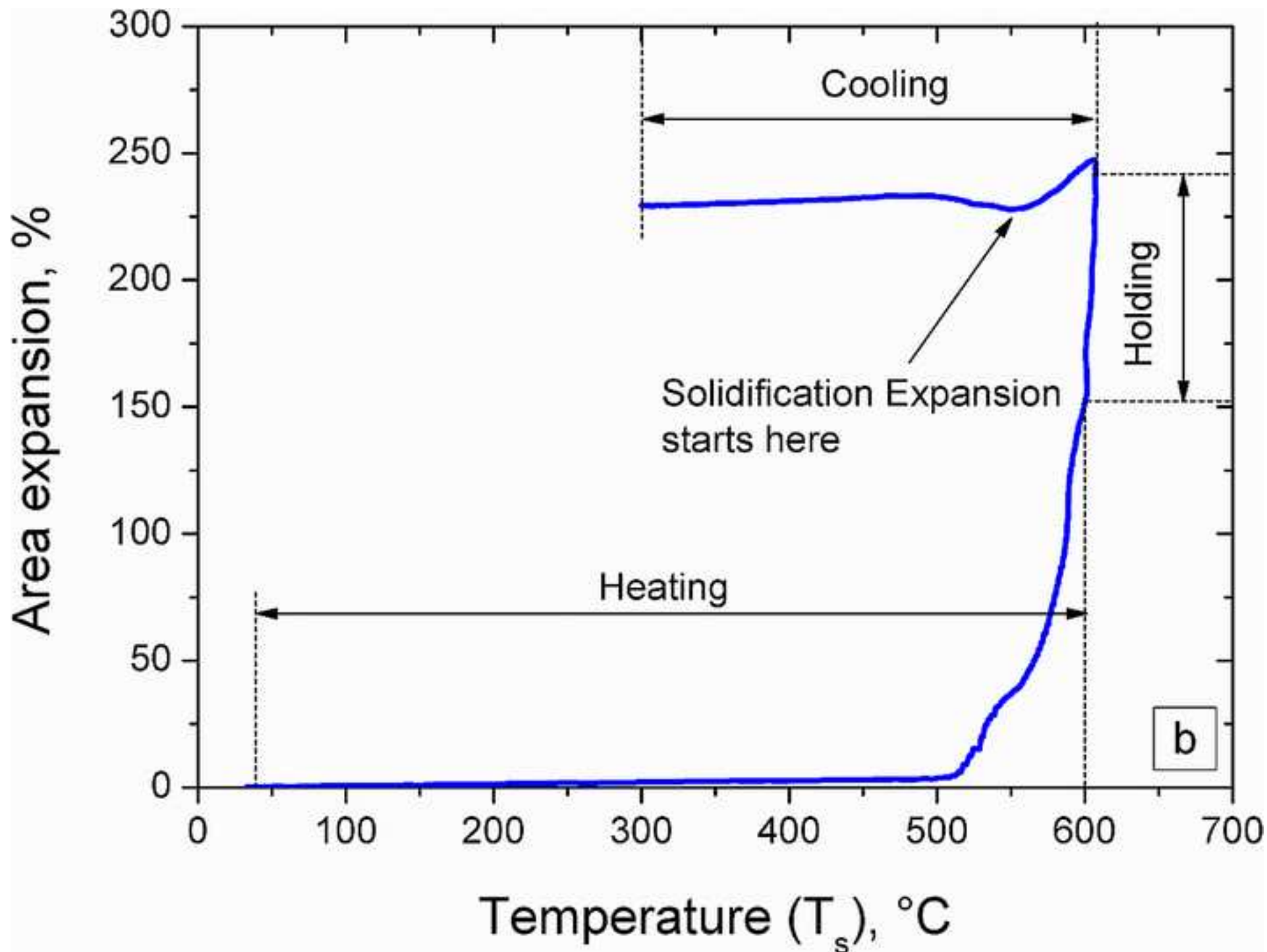


Figure 2
[Click here to download high resolution image](#)

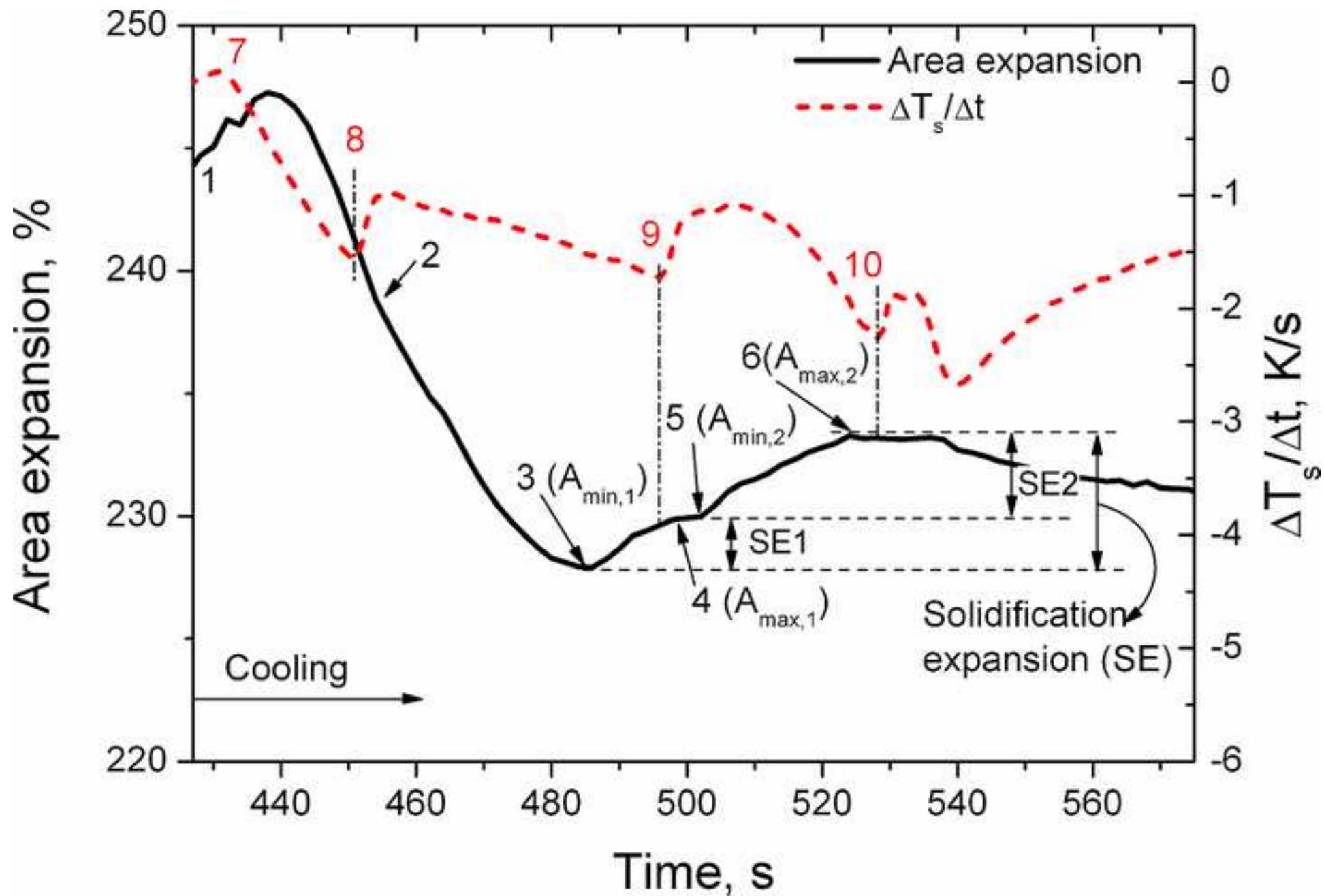


Figure 3
[Click here to download high resolution image](#)

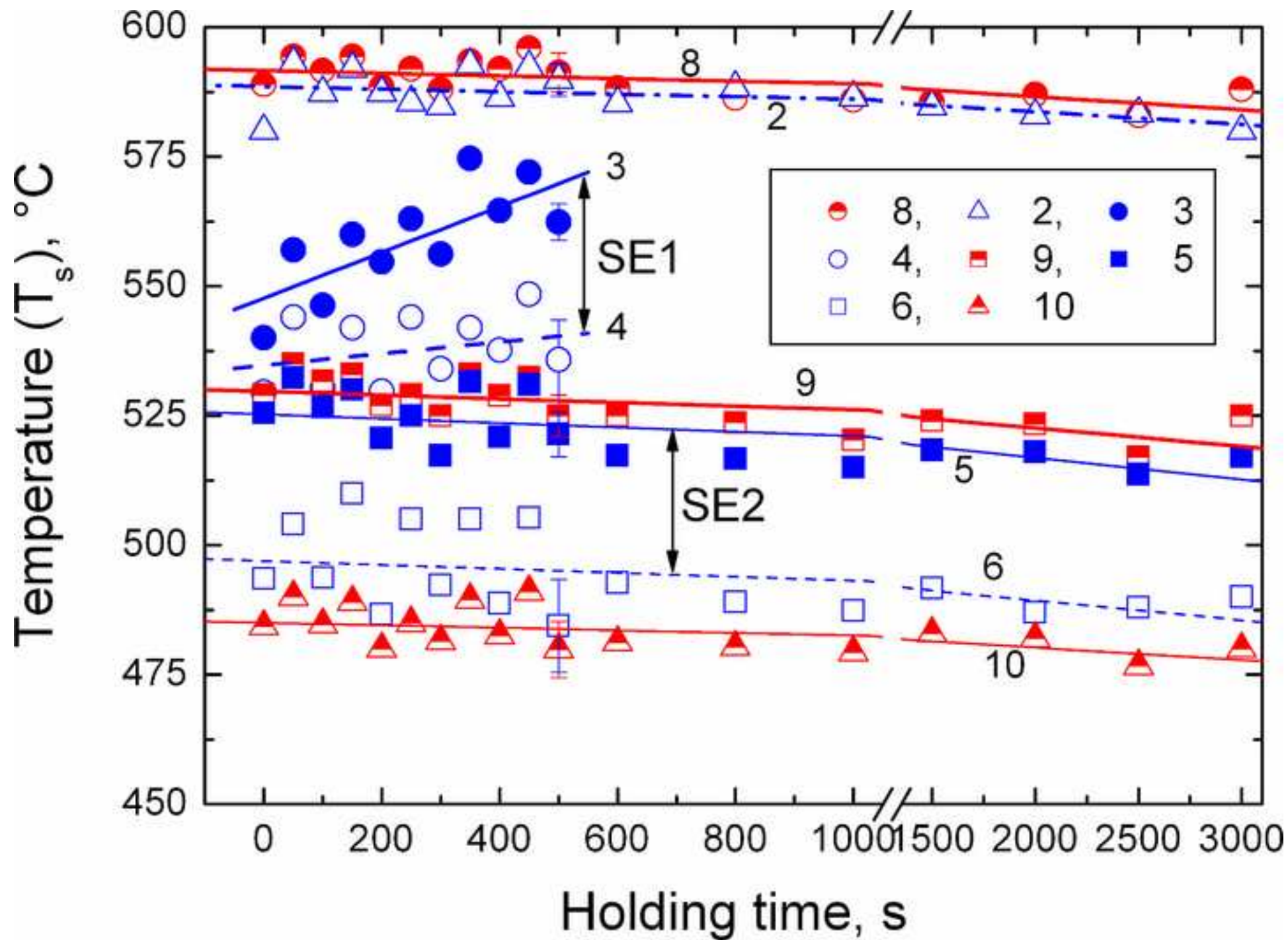


Figure 4(a)
[Click here to download high resolution image](#)

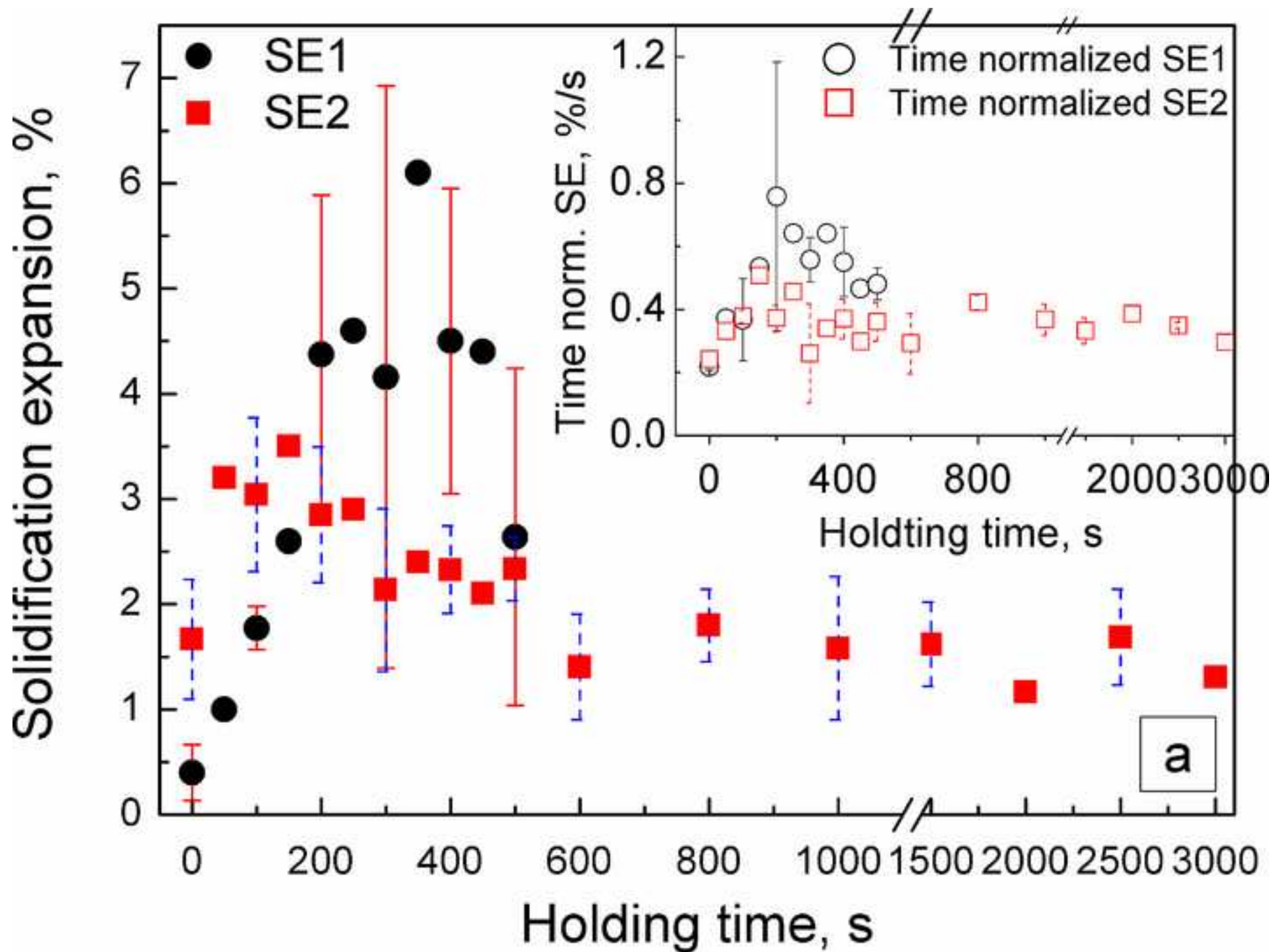


Figure 4(b)
[Click here to download high resolution image](#)

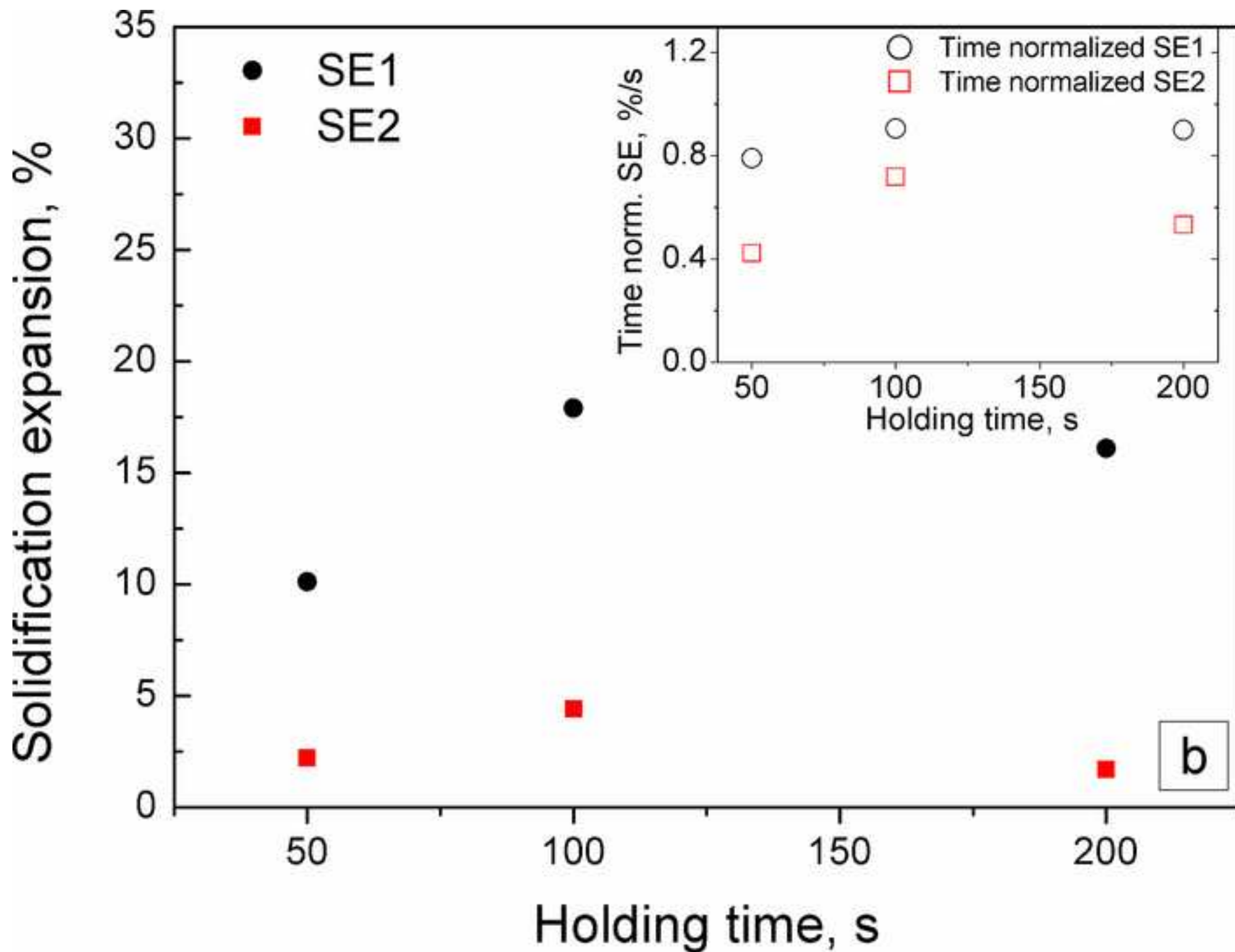


Figure 5(a)

[Click here to download high resolution image](#)

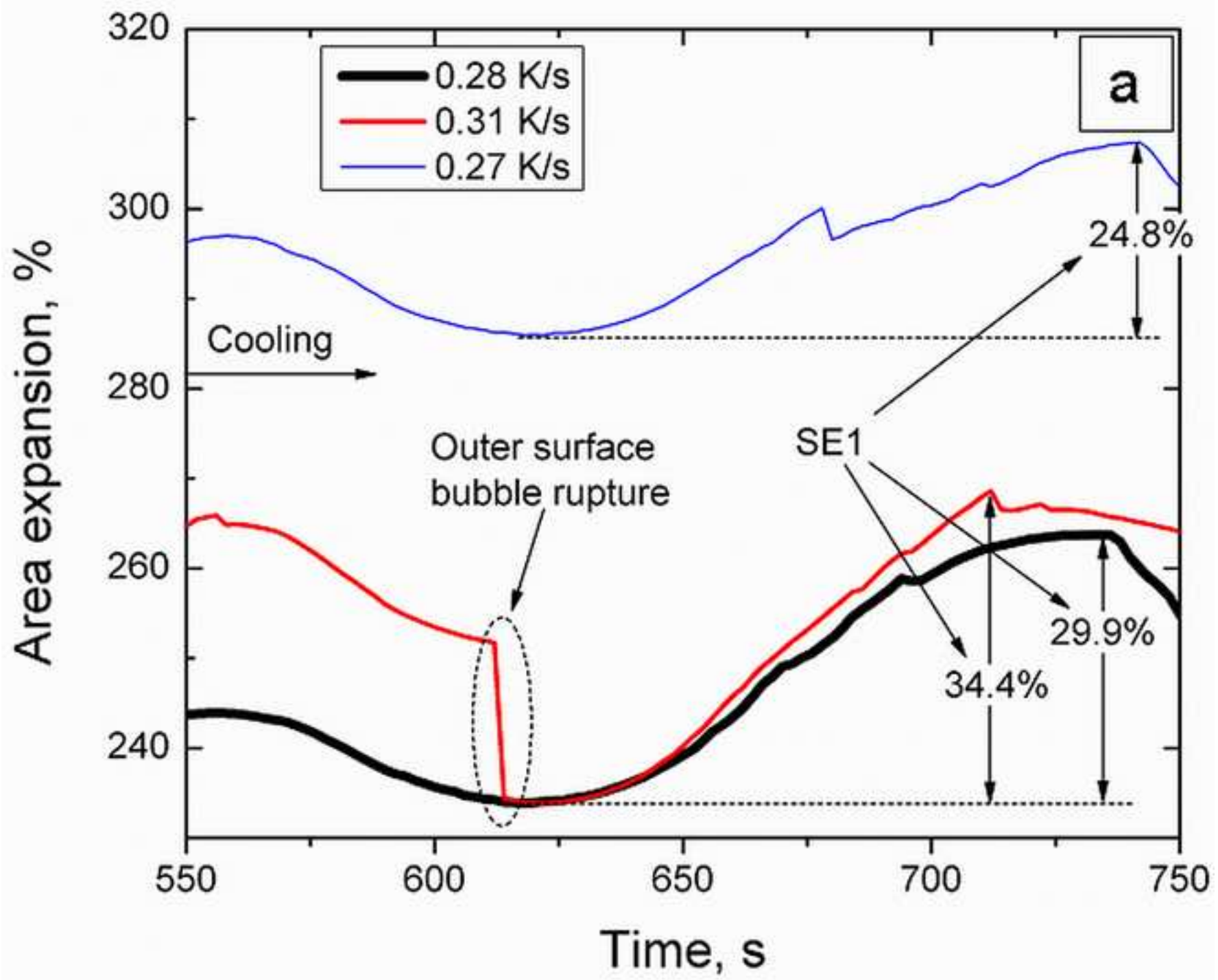


Figure 5(b)
[Click here to download high resolution image](#)

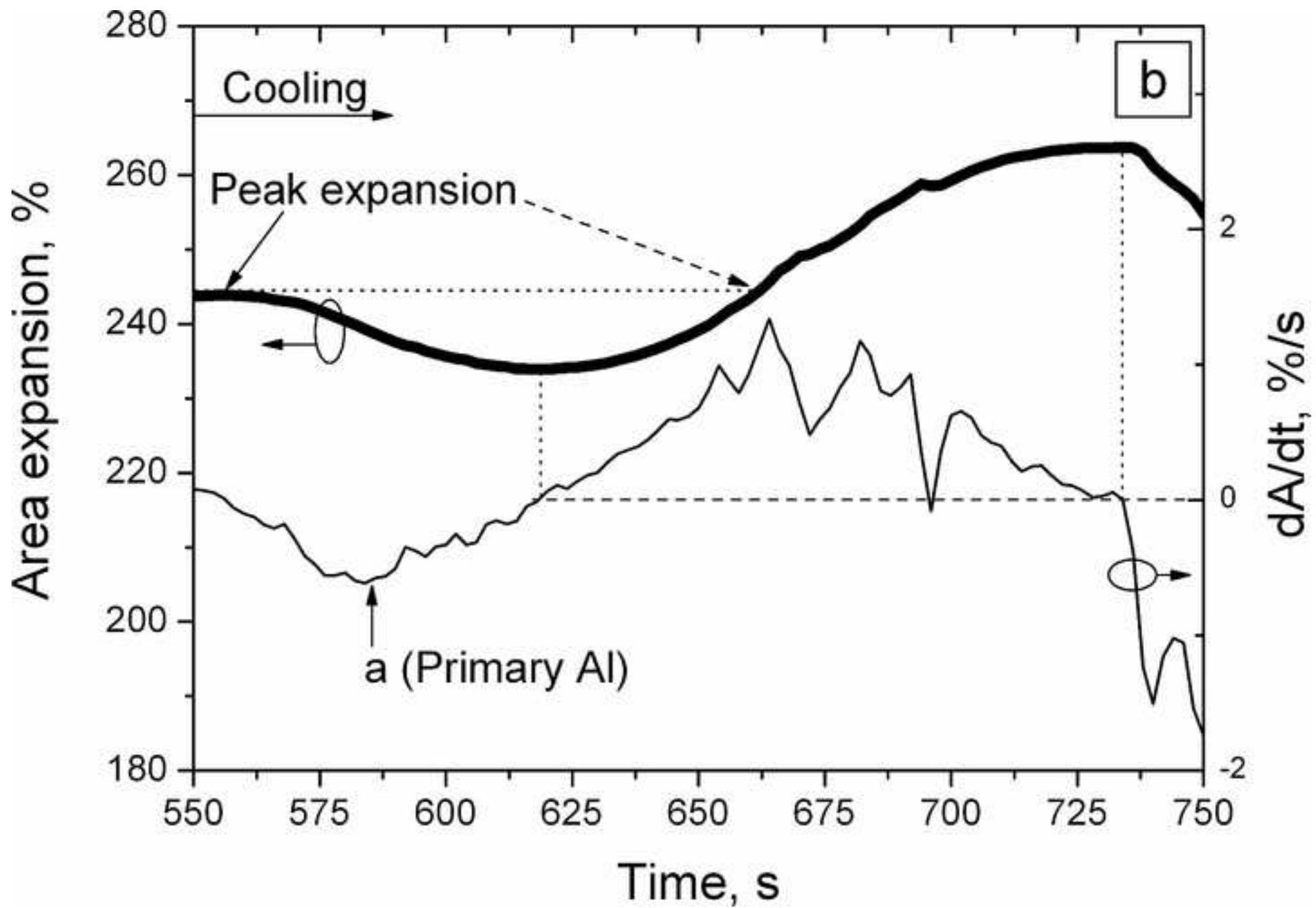


Figure 6(a)
[Click here to download high resolution image](#)

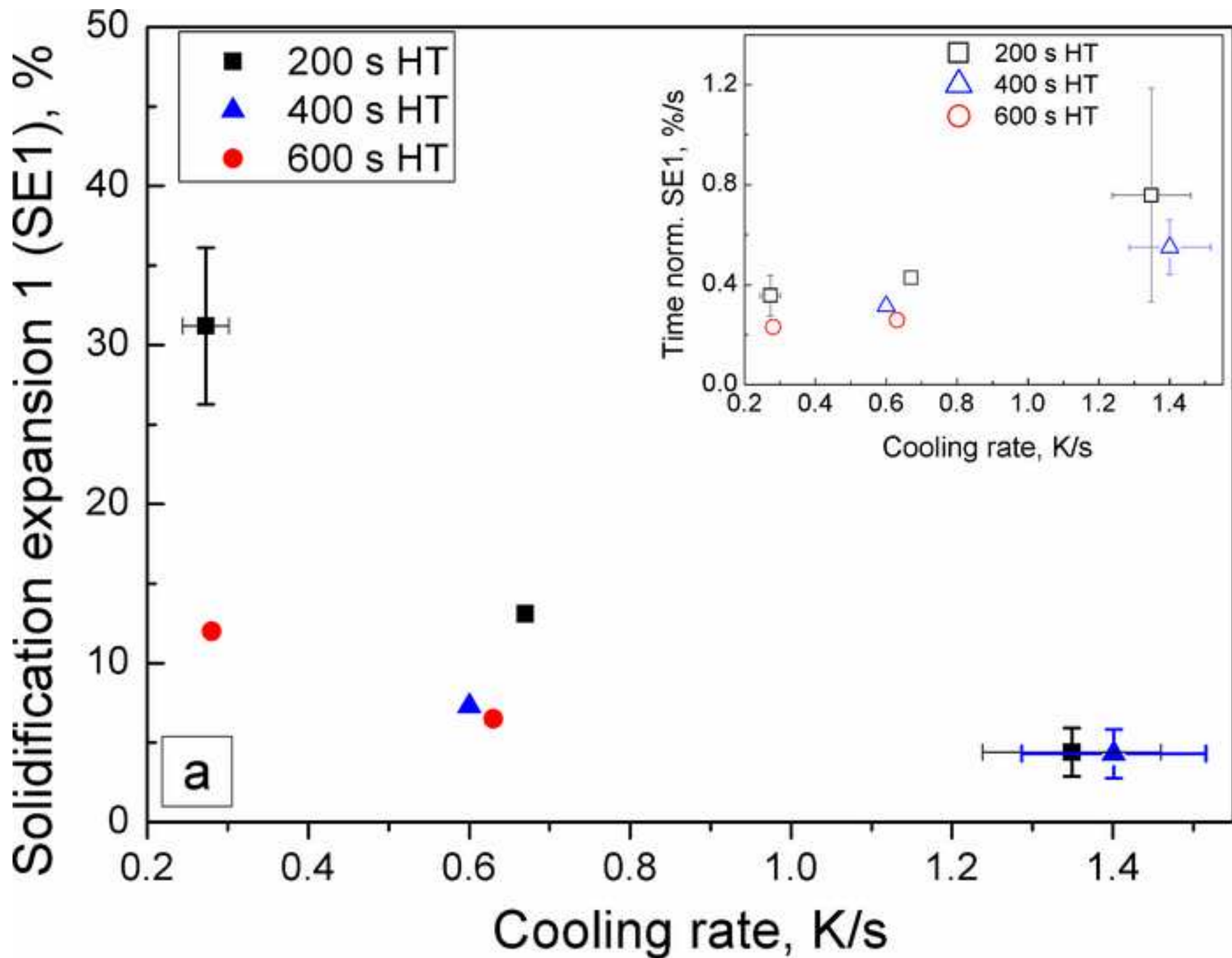


Figure 6(b)
[Click here to download high resolution image](#)

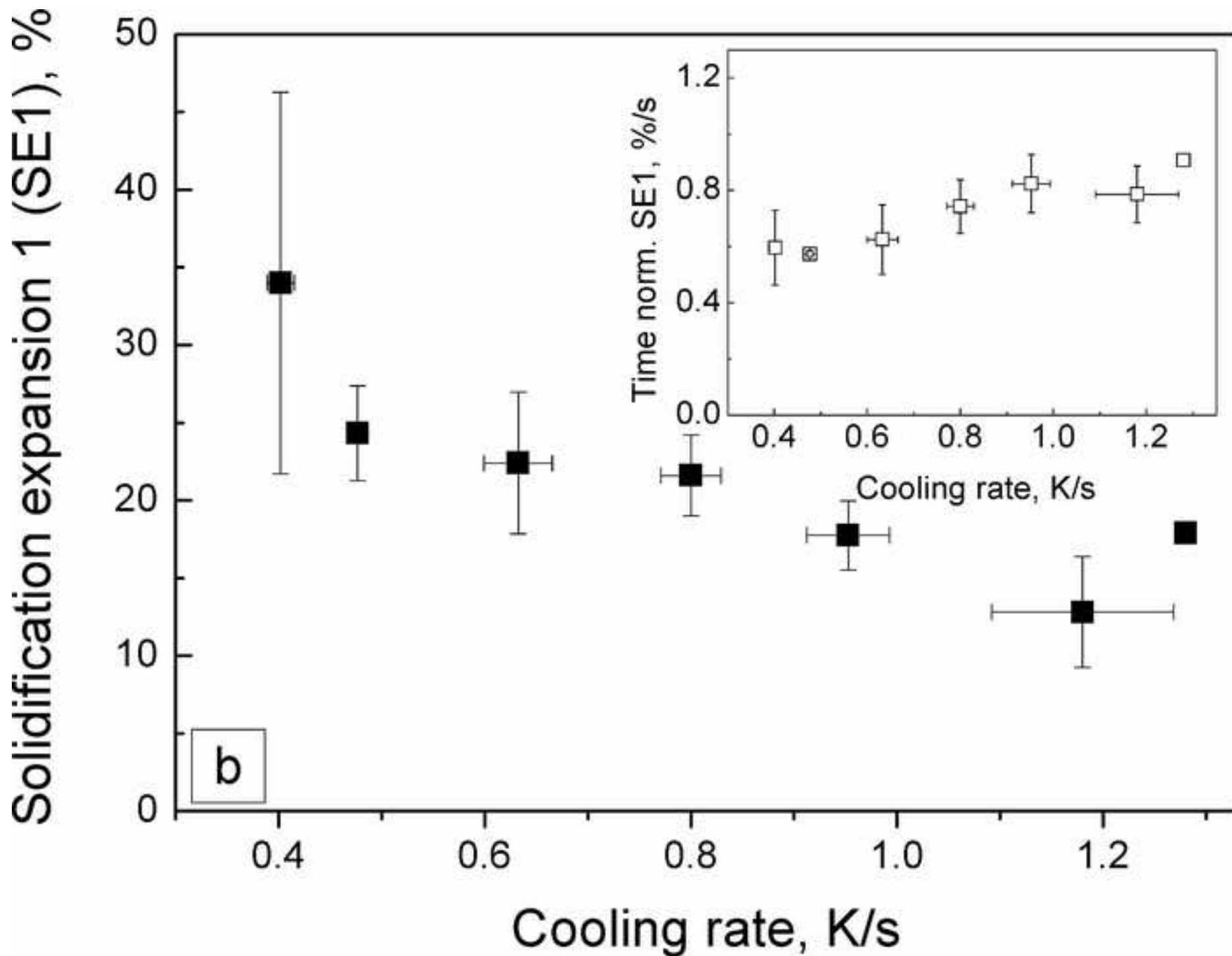


Figure 7
[Click here to download high resolution image](#)

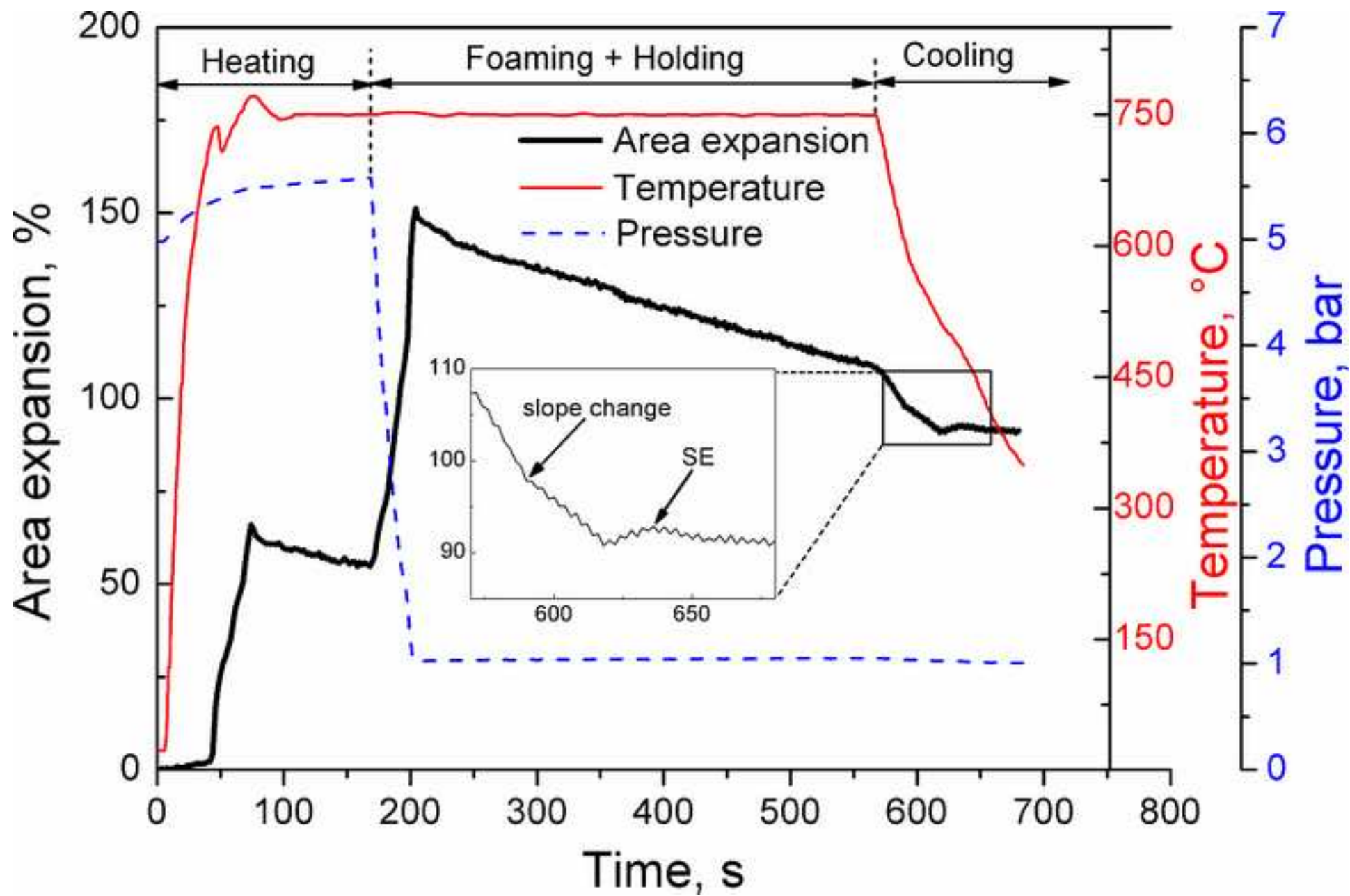


Figure 8(a)
[Click here to download high resolution image](#)

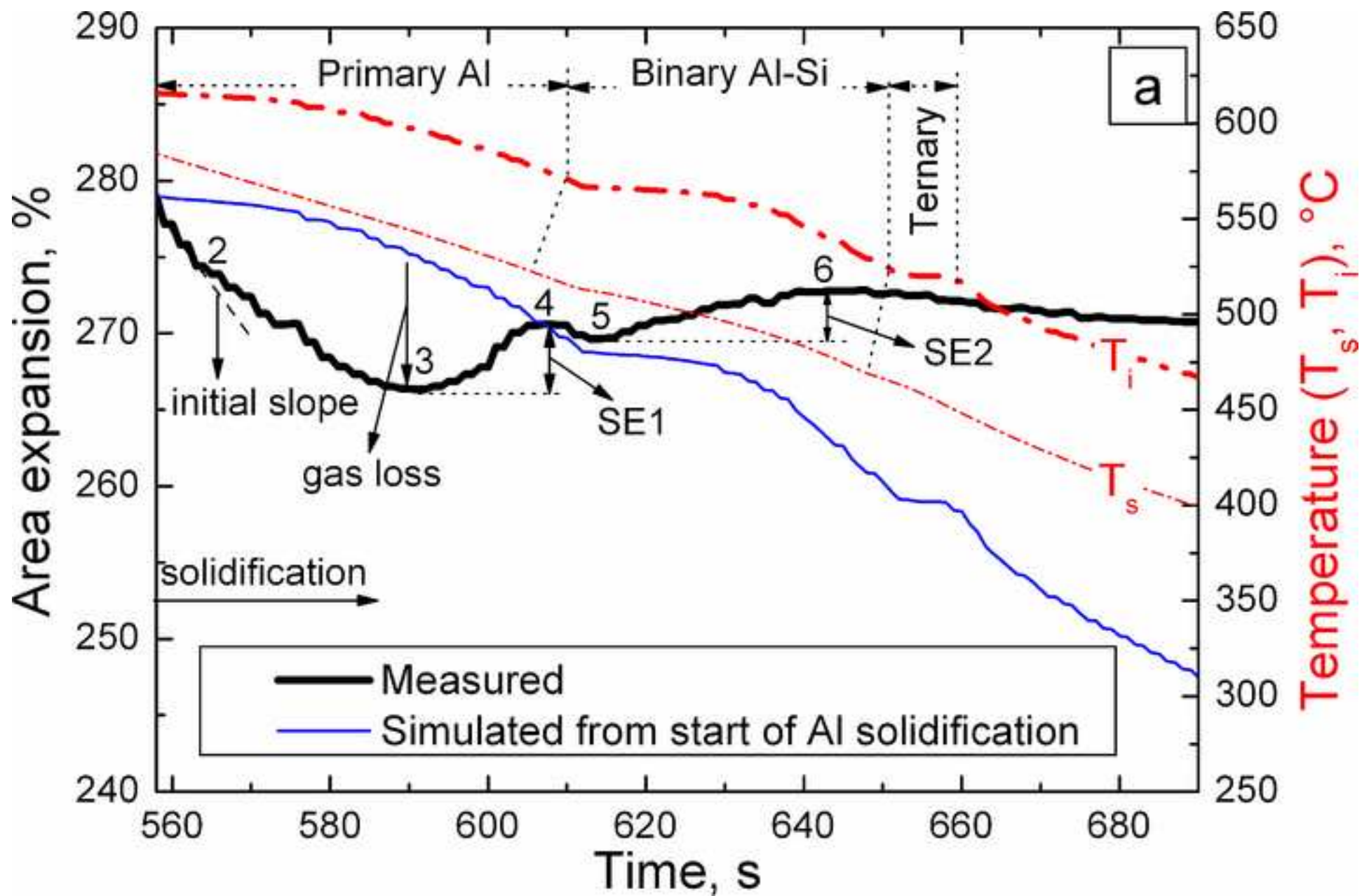


Figure 8(b)
[Click here to download high resolution image](#)

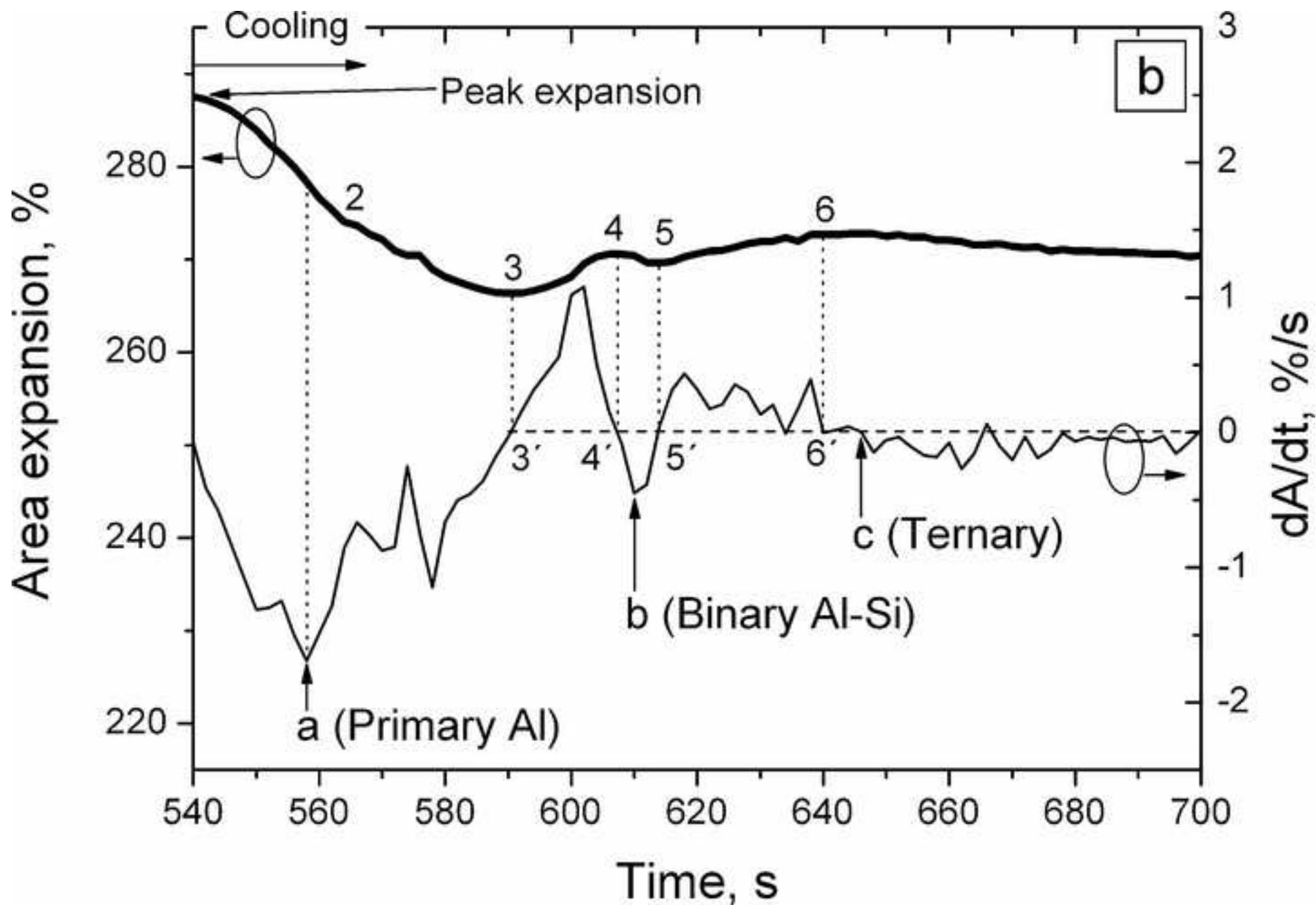


Figure 9
[Click here to download high resolution image](#)

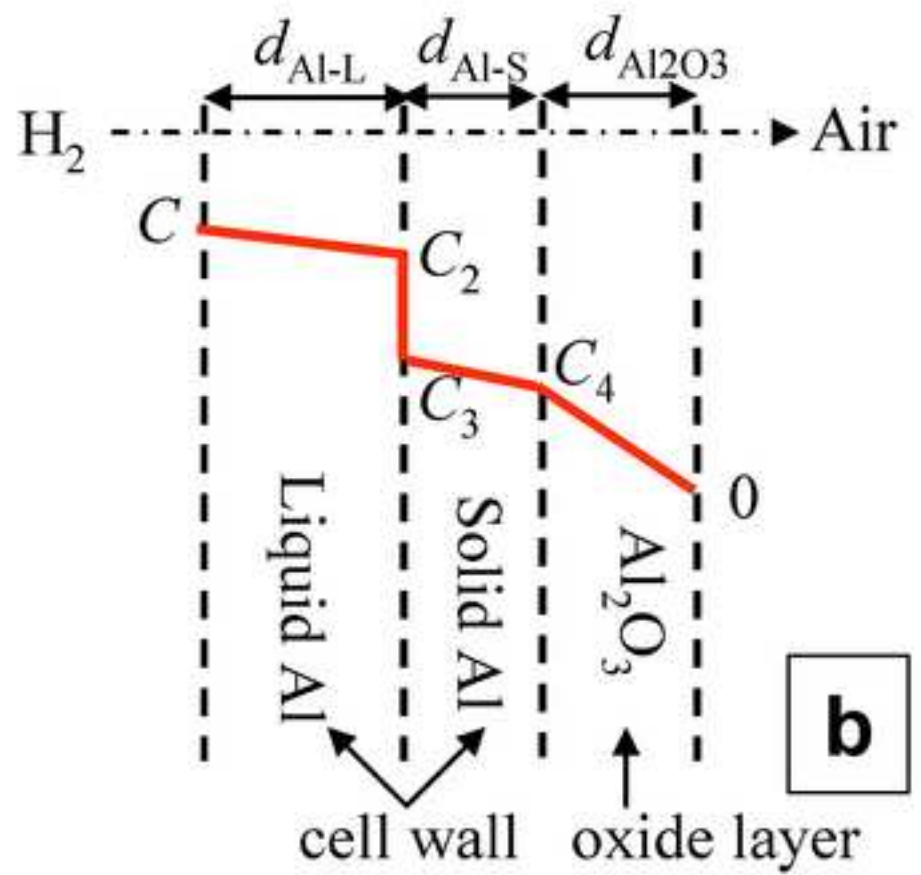
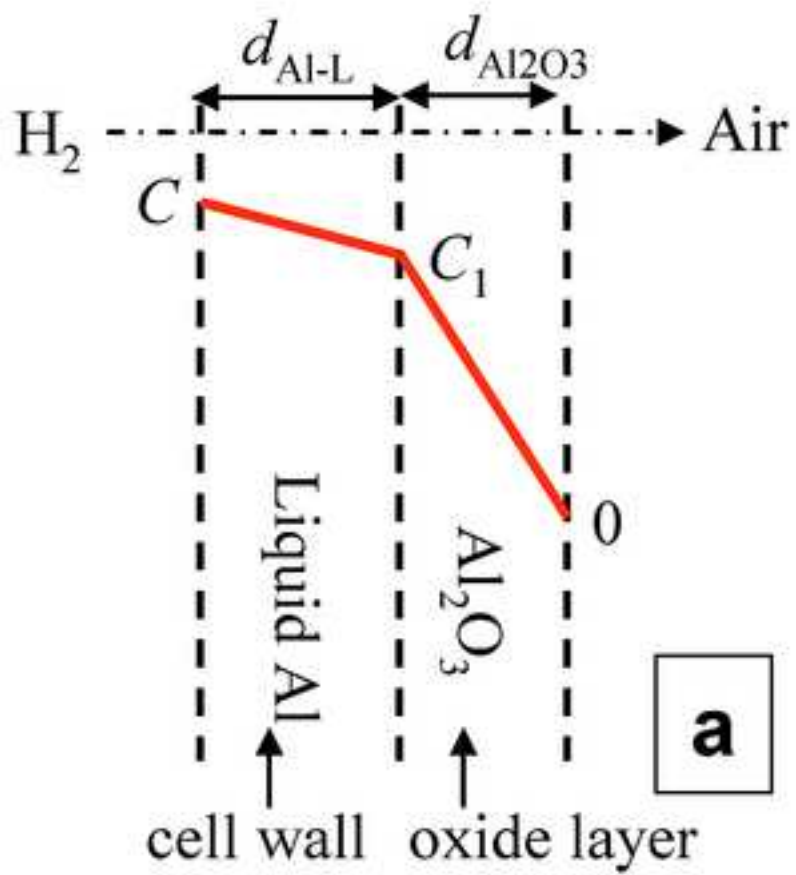


Figure 10
[Click here to download high resolution image](#)

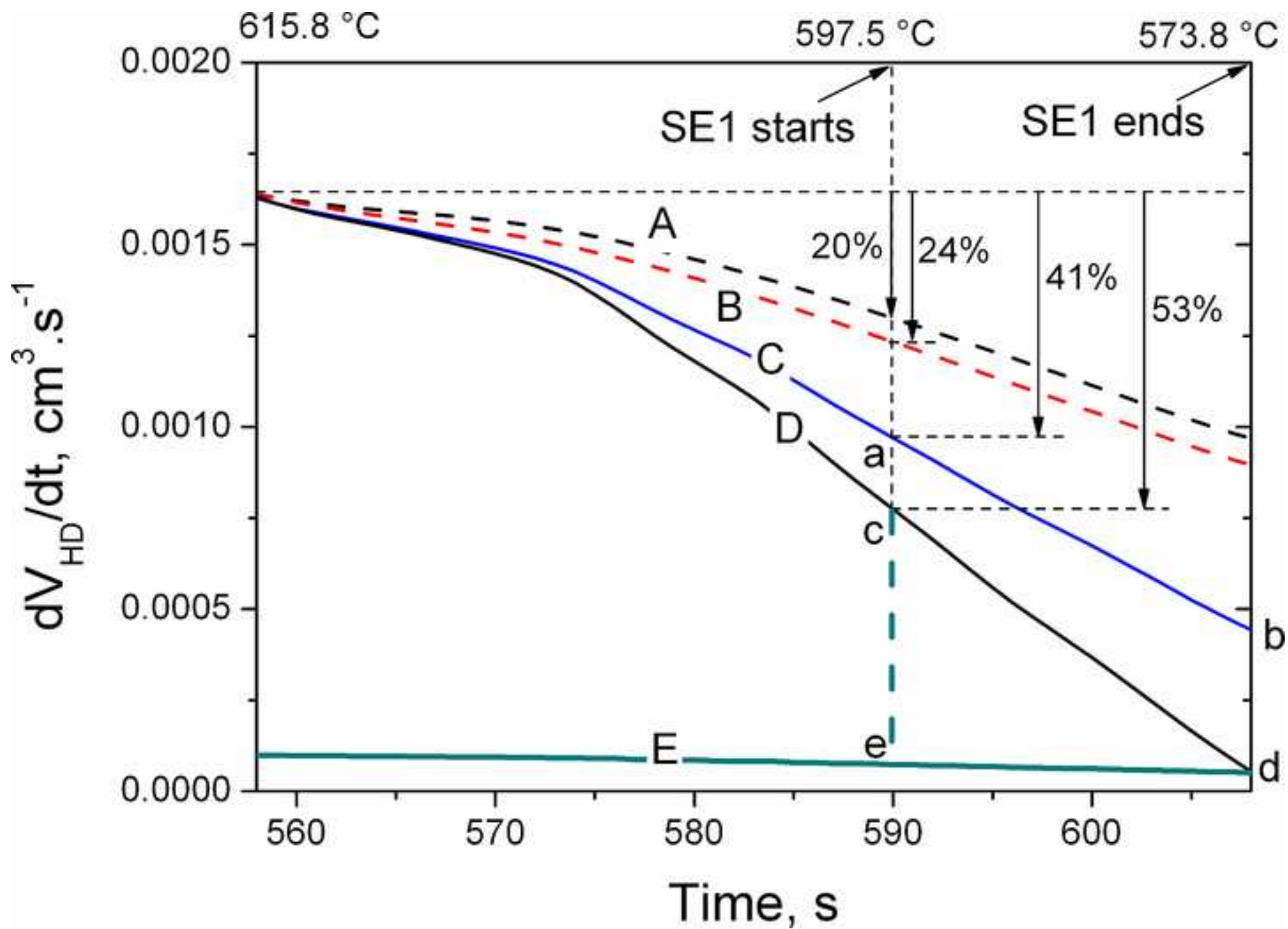


Figure 11
[Click here to download high resolution image](#)

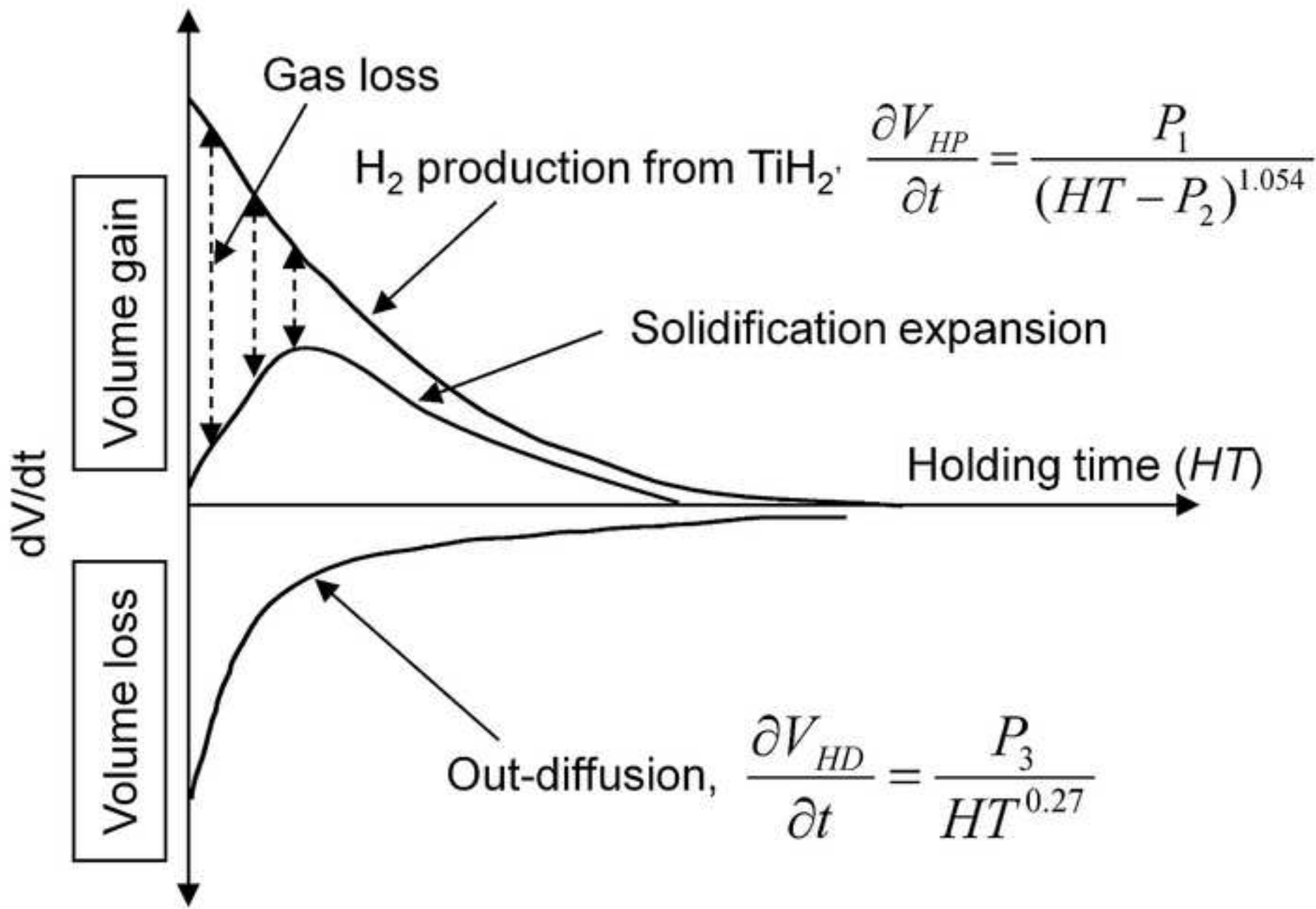


Figure 12
[Click here to download high resolution image](#)

